AD-A142 393 ELASTIC DOMAIN WALL WAVES IN FERROELECTRIC CERAMICS AND SINGLE CRYSTALS(U) STANFORD UNIV CA EDWARD L GINZTON LAB OF PHYSICS B A AULD APR 84 GL-3716 1/1

UNCLASSIFIED N00014-79-C-0222 F/G 20/2 NL

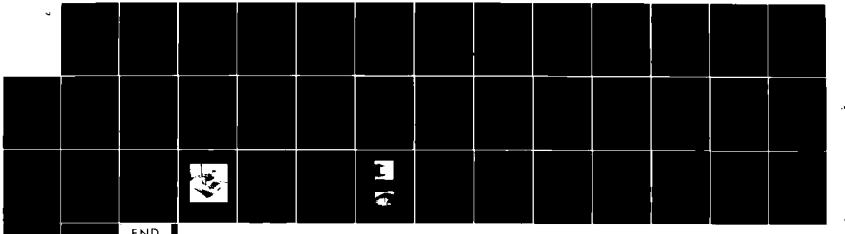

END
DATE FILMED
8-84
DTIC

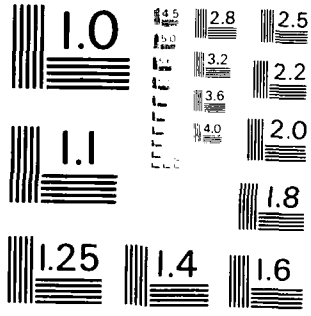

(12)

ELASTIC DOMAIN WALL WAVES IN FERROELECTRIC CERAMICS AND SINGLE CRYSTALS

Annual Progress Report

1 February 1983—31 January 1984

Contract No. N00014-79-C-0222

G. L. Report No. 3716

April 1984

Principal Investigator

B. A. Auld

Edward L. Ginzton Laboratory
W. W. Hansen Laboratories of Physics
Stanford University
Stanford, California 94305

UNCLASSIFIED

SECURITY CLASSIFICATION OF THIS PAGE (When Data Entered)

REPORT DOCUMENTATION PAGE		READ INSTRUCTIONS BEFORE COMPLETING FORM
1. REPORT NUMBER	2. GOVT ACCESSION NO. AD-A142 343	3. RECIPIENT'S CATALOG NUMBER
4. TITLE (and Subtitle) ELASTIC DOMAIN WALL WAVES IN FERROELECTRIC CERAMICS AND SINGLE CRYSTALS		5. TYPE OF REPORT & PERIOD COVERED Annual Progress Report 1 Feb. 1983 - 31 Jan. 1984
		6. PERFORMING ORG. REPORT NUMBER G.L. Report No. 3716
7. AUTHOR(s) B. A. Auld		8. CONTRACT OR GRANT NUMBER(s) N00014-79-C-0222
9. PERFORMING ORGANIZATION NAME AND ADDRESS Edward L. Ginzton Laboratory W.W. Hansen Laboratories of Physics Stanford University, Stanford, Ca. 94305		10. PROGRAM ELEMENT, PROJECT, TASK AREA & WORK UNIT NUMBERS
11. CONTROLLING OFFICE NAME AND ADDRESS Director, Metallurgy and Ceramics Program Office of Naval Research 800 N. Quincy St., Arlington, VA 22217		12. REPORT DATE April 1984
		13. NUMBER OF PAGES 42
14. MONITORING AGENCY NAME & ADDRESS (if different from Controlling Office)		15. SECURITY CLASS. (of this report)
		15a. DECLASSIFICATION/ DOWNGRADING SCHEDULE

16. DISTRIBUTION STATEMENT (of this Report)

Approved for Public Release - Distribution Unlimited

17. DISTRIBUTION STATEMENT (of the abstract entered in Block 20, if different from Report)

18. SUPPLEMENTARY NOTES

19. KEY WORDS (Continue on reverse side if necessary and identify by block number)

Piezoelectricity	Biased Transducers
Composites	Surface Waves
Space Harmonics	Attenuation
Kaser Probe	Brillouin Zone
Electrostrictors	PZT-epoxy

20. ABSTRACT (Continue on reverse side if necessary and identify by block number)

More detailed measurements have been made on the resonance mode structure of PZT-composite plate transducers. These are compared with constant strain and constant stress versions of Floquet (space harmonic) theory, with good agreement. Quantitative measurement procedures for measuring bulk wave and surface wave coupling in PMN are being developed. The dependence of poled interface waveguide characteristics on fabrication parameters have been measured, and interface waveguide directional couplers have been realized.

DD FORM 1 JAN 73 1473 EDITION OF 1 NOV 65 IS OBSOLETE

UNCLASSIFIED

SECURITY CLASSIFICATION OF THIS PAGE (When Data Entered)

CONTENTS

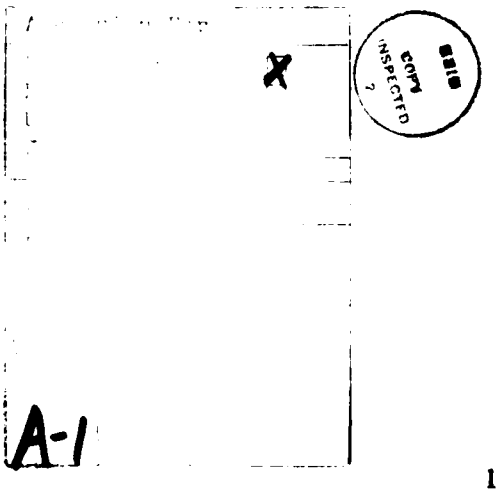

I. INTRODUCTION

The general scope of this project is to investigate properties of ferroelectric ceramics using new measurement techniques and to look for new technological uses of these materials in device applications. One main focus of the effort is a study of interfaces between counterpoled regions of a ferroelectric ceramic. Such counterpoled ceramics have been used in the past for focused Fresnel zone plate transducers, bimorphs and tuning fork resonators. In such applications it is important to know the structure of the interface and how it relates to material composition and history.

Powerful techniques for experimental study of these questions involve: (1) elastic wave scattering by an interface, (2) elastic wave guidance along an interface, (3) laser probe pyroelectric measurements of the electric polarization profile through an interface, (4) laser probe measurements of the mechanical vibration profile through an interface. Items (1) and (2) lead to potential device applications in the form of grating filters and interface delay lines. A theoretical basis for treating uniform arrays of interfaces, such as might be used in these devices, requires a general analysis of high frequency elastic wave propagation in spatially periodic media. Such a theory can be constructed by using space harmonic analysis, as developed for the vibration spectra of crystal lattices, and is also applicable to periodicities in one-, two- or three-dimensional dimensions. These multidimensional periodicities occur in a variety of PZT-epoxy composite materials, and a theory of elastic wave propagation is of fundamental importance in understanding this class of ferroelectric materials.

The material interfaces discussed above may be introduced *extrinsically* by inserting actual material inclusions in a matrix medium (as in the case of the family of PZT-epoxy composite transducer materials), or *intrinsically* by altering the material properties with selectively applied spatial distributions of electric field bias. In the second case, one can distinguish between: (1) intrinsic material inhomogeneities introduced by poling patterns of electrical polarization into remanent-type ferroelectrics (such as PZT or PLZT), and (2) intrinsic inhomongeneities introduced by selective electric field biasing of relaxor-type ferroelectrics (such as PMN). Materials with intrinsic inhomogeneities offer exciting possibilities for realizing a variety of planar signal routing and processing devices on small ferroelectric wafers, fabricated by simple inexpensive poling and biasing techniques. Such devices may be either slowly or rapidly switched and programmed, according to the choice of either a remanent-type or a relaxor-type ferroelectric material.

II. COMPOSITE RESONATOR AND TRANSDUCER STUDIES

These studies are being pursued in collaboration with R.T. Gururaja, W.A. Schulze and L.E. Cross at the Materials Science Laboratory of the Pennsylvania State University, and with Dr. W. Smith at the Philips Research Laboratory. The initial goal was to investigate the high frequency dynamic behavior of 3:1 connected PZT-epoxy composites in plate transducer configurations, to better understand the physics of these materials, and to explore their exploitation for applications other than hydrophones. Progress made in formulating a general Floquet (or space harmonic expansion) theory of elastic vibrations in composites now makes it possible to extend the goals of this research. The dynamic behavior of composite materials consisting of *general* periodic lattices of inclusions in a matrix can be analysed using this theory, which has been tested in certain specific configurations against experimental results. A capability now exists for quantitatively studying and exploiting periodic composite materials (whether piezoelectric or nonpiezoelectric) in meeting Navy needs for improved, more reliable and cost-effective techniques for detecting, generating, and controlling acoustic vibrations in liquids and solid structures—including specifically the development of anechoic structures and the control of undesirable noise in detectors.

A. Theory

Basic features of the theory were outlined in the Annual Progress Report for 1 February 1982–31 January 1983, and initial encouraging comparisons with experiment were reported there. During the year covered by the present report, these results were refined and compared in more detail with electrical transducer impedance measurements, time delay measurements of acoustic velocity, and laser probe vibration pattern measurements.[1–3] References 1 to 3 described the theory for unbounded isotropic composites with two-dimensional periodicity in the xy plane (summarized in Appendix A). Explicit calculations have been made for the "superlattice" unit cell geometries shown in Fig. 1.

Although the general formulation is capable of treating Floquet waves propagating in arbitrary directions, attention was initially focused on wave propagation either normal to the plane of the periodicity (xy-plane) or parallel to that plane. These propagation directions correspond, in the first case, to the longitudinal thickness resonances of a composite transducer and, in the second case, to lateral resonances of the transducer. Lateral resonances occur in all transducers.[4] However, certain resonances in composite transducers are enhanced by Bragg-scattering from the lateral periodicity, and by phase-matched coupling of the electrical excitation to selected lateral resonances through the periodically distributed piezoelectric coupling.

Figure 2(a) gives a typical input impedance versus frequency curve, measured on a Penn

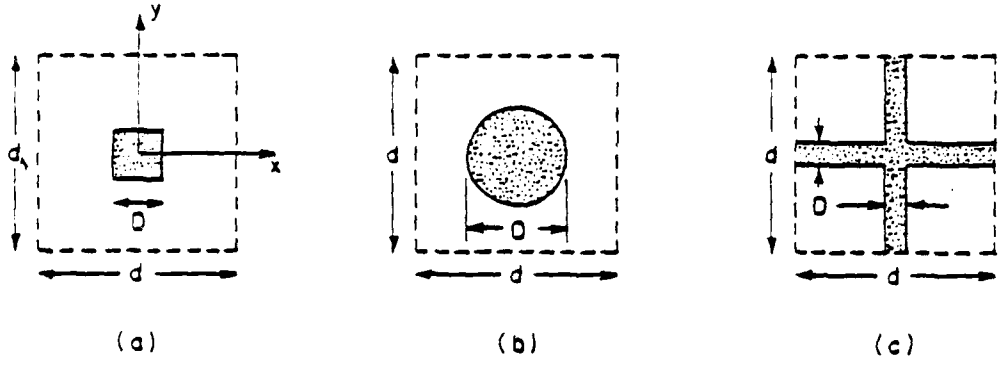

FIGURE 1

Two-dimensional unit cell geometries. Area of unit cell is A. Area of PZT (shaded) is a.

State sample and showing three strong resonances. Here, f_ℓ is the longitudinal thickness resonance and f_{t1}, f_{t2} are the two dominant lateral standing wave resonances—along the unit cell edge and the unit cell diagonal, respectively (Fig. 2(b)). Since the sample is uniformly electroded, the piezoelectric elements (shown stippled in Figs. 1 and 2(b)) are driven in phase, so that the elastic vibrations excited must also be in phase at these points. This means that the lateral resonances observed in Fig. 2(a) consist of standing waves with one full-wavelength spacing between the piezoelectric elements—along the unit cell edge for f_{t1} and along the unit cell diagonal for f_{t2}. Such standing wave patterns are shown schematically in Fig. 3 ((a) for f_{t1} and (b) for f_{t2}). These patterns will be discussed more fully in Section II.B below, in connection with laser probe measurements of the motion of composite resonators.

Our study of lateral resonances in composite transducers was initially approached by assuming wave propagation in the xy-plane of an infinite composite. The model was further simplified by supposing that only a z-polarized elastic displacement existed, reducing the elastic wave function to a scalar form similar to that appearing in electronic band theory. In a first approximation, coupled mode theory (which retains only simultaneously "resonant" space harmonics) is used to find the edges of the stop bands for wave propagation in the composite medium. Stopband edges are located at frequencies where Bragg-scattering resonances occur between certain planes of PZT rods (Bragg planes) in the periodic array of rods. (Resonances occur at frequencies for which the Bragg planes are spaced by integral multiples of $\lambda/2$ for

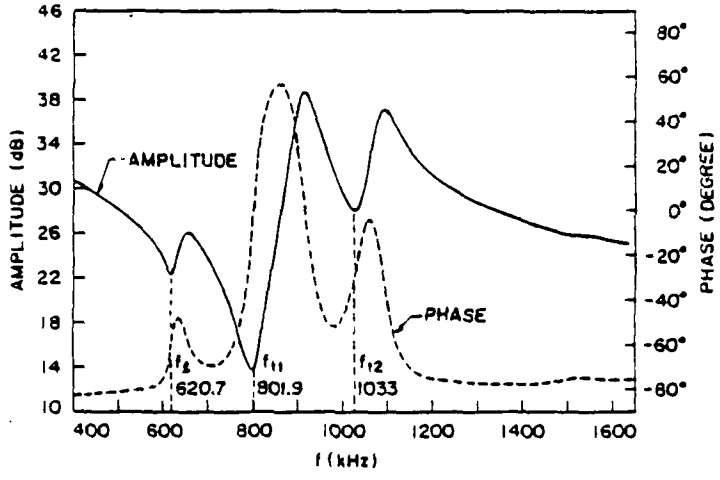

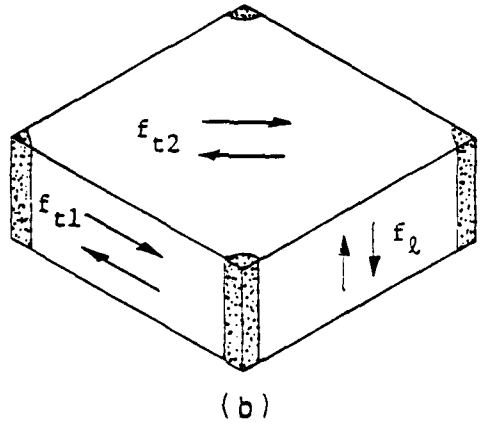

FIGURE 2

Resonance spectrum of a periodic composite plate resonator: (a) Typical measured impedance curve; (b) Corresponding standing wave patterns.

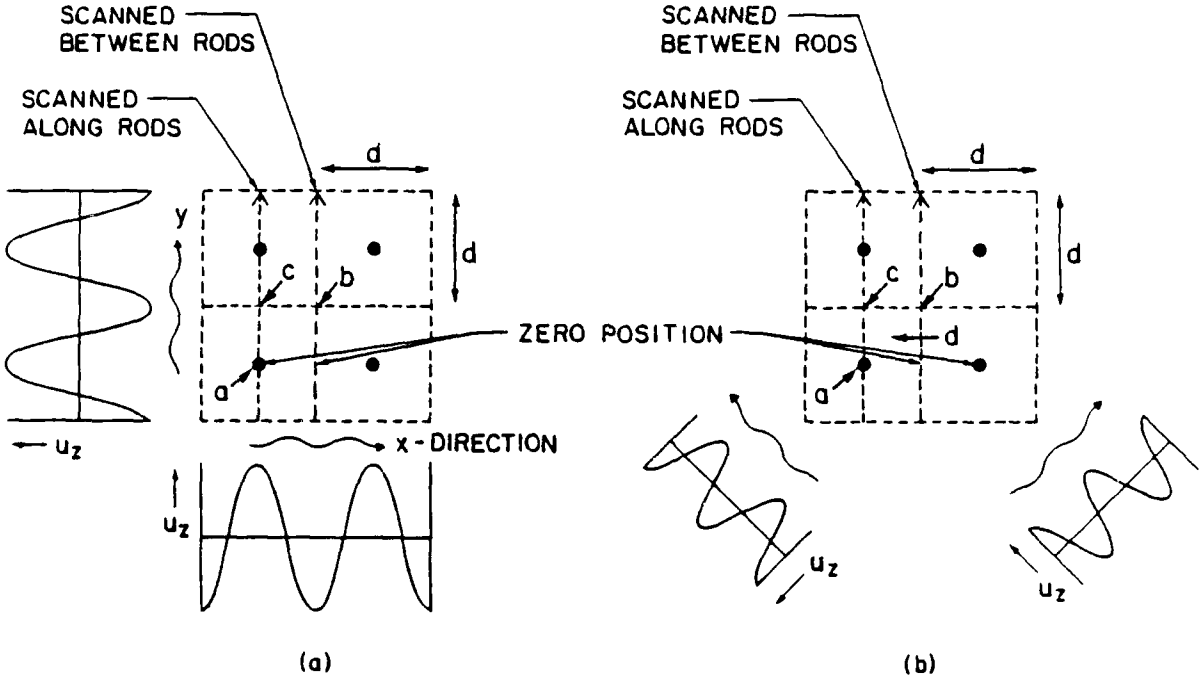

FIGURE 3

Unit cell geometries and laser scan paths for $d = \lambda$ Bragg resonances: (a) Standing waves along cell edge (f_{t1}); (b) Standing waves along cell diagonal (f_{t2}).

the z-polarized shear wave assumed in the model.) These "Bragg" resonances are just the enhanced lateral resonances referred to above.

At $\lambda/2$ spacing between the Bragg planes, the resonant wave functions are standing waves along the unit cell edge, the unit cell diagonal, and perpendicular to the higher Bragg planes. These resonances cannot, however, be excited piezoelectrically in a uniformly electroded sample because neighboring PZT rods vibrate 180° out of phase. The lowest lateral mode that can be excited piezoelectrically in this geometry is that which occurs when the edge of the unit cell equals one full wavelength (f_{t1} in Fig. 2). At this resonant frequency several allowed Bragg-scattering resonances occur, but only the mode shown in Fig. 3 has the PZT rods all vibrating in phase.[3] For the longitudinal thickness resonance (f_ℓ in Fig. 2), Bragg-scattering resonances do not appear, because there is no periodicity of the medium along the z-propagation direction. In this case the simplest model is a z-propagation longitudinal wave with properties determined by $\overline{\rho}$ and $\overline{c}_{33}$ (spatial averages over the unit cell), and with weakly excited space harmonics because no resonance of the space harmonics can occur. In other words, the Bragg-scattering condition cannot be satisfied.

Comparison of experimentally measured resonant frequencies with those calculated from the simple model described above gives good agreement for the longitudinal thickness mode but only fair agreement for the lateral modes.[1]. One reason for this is that the theory uses a spatial average of the density and the elastic stiffness constants c_{IJ} (see Eqs. (2)-(4) in Appendix A) to model the effective properties of the medium at low frequencies, where scattering from the periodicity is unimportant. This corresponds to the *constant strain model* for the static (or low frequency) behavior of a composite. If a particular strain component (the J-th) has the same value (S_J) in the plastic matrix and in the PZT rod, the average I-th component of stress over the unit cell is (see Fig. 1)

$$\left(\frac{(A-a)(c_{IJ})_{plastic}+a(c_{IJ})_{PZT}}{A}\right)S_J=\overline{c}_{IJ}S_J\,, \tag{1}$$

corresponding to the spatial averaging of the stiffness c_{IJ} in Eq. 3(a) of Appendix A. For the longitudinal thickness resonance (f_ℓ) the plastic matrix and the PZT rods vibrate like springs in parallel, and the model of Appendix A reduces to this constant strain description at low frequencies.

For the lateral resonances in Fig. 2(b), the plastic and the PZT are elastic members connected in series, so that the stress (not the strain) is common to both; and the low frequency behavior of the medium is best represented by the *constant stress model*. In this case the counterpart of Eq. (1) is

$$\left(\frac{(A-a)(s_{IJ})_{plastic}+a(s_{IJ})_{PZT}}{A}\right)T_J=\overline{s}_{IJ}T_J\,, \tag{2}$$

for the average strain over the unit cell. Vibrations of the composite material at low frequencies are now most accurately calculated from the spatially averaged compliances $\bar{s}_{IJ}$, rather than the $\bar{c}_{IJ}$ of Appendix A.

Another reason for the observed discrepancies between experiments and the theory of Appendix A is that the stress-free boundary conditions at the surfaces of the plate have not been considered. This point was discussed briefly in Reference 2. It was noted there that additional coupling among the space harmonics occurs at the boundaries, and that new plane wave terms (not contained in the original set of space harmonics) are also generated by elastic mode boundary coupling.

Appendix A (excerpted from Reference 3) summarizes the Floquet theory of wave propagation in an infinite isotropic elastic composite with two-dimensional periodicity. This theory is not adequate for a complete treatment of the composite plate transducer problem, because it does not include plate boundary conditions. As was noted in the previous paragraph, the addition of boundary conditions to the theory of Appendix A introduces a number of complications. Several attempts have been made to follow this approach. However, it was found that (because of additional boundary couplings introduced between space harmonic orders and between different polarizations of the same space harmonic order) this is not a useful way to implement the coupled mode approximation for composite plates or to iterate the coupled approximation up to solutions of increased accuracy.

A solution to the above difficulty is found by taking the basis functions of the Floquet solution to be Lamb and SH waves of the plate, rather than plane waves. This procedure has been carried out in detail for the case of a composite plate with material parameter periodicity along one direction (x) only (Fig. 4). Details of the analysis are given in Appendix B, where the general set of coupled space harmonic amplitude equations is shown to be of the form

$$(\omega - \omega_{m\mu})a_{m\mu} = \omega \sum_{n\nu} K_{m\mu,n\nu} a_{n\nu} \tag{3}$$

In Eq. (3) m, n are one-dimensional space harmonic indices, and μ, ν are Lamb mode indices. (For a one-dimensional periodicity, the Lamb and SH wave solutions are separable by symmetry. The case of two-dimensional periodicity can also be treated by the same method). Using Eq. (3), the coupled-mode approximation is easily implemented by selecting only the near "resonance" terms on the left-hand side. However, it must be noted that, in these equations, simultaneous "resonance" (Bragg-scattering) may occur *either* between space harmonics of the *same* Lamb wave species, *or* between space harmonics of *different* Lamb wave species. This adds a great many stop bands in the wave dispersion curves. Nevertheless, the Lamb wave approach of Appendix B, as distinct from the plane wave approach of Appendix A, does give a clear-cut method for describing and studying the stop band (or resonance) structure of the composite plate.

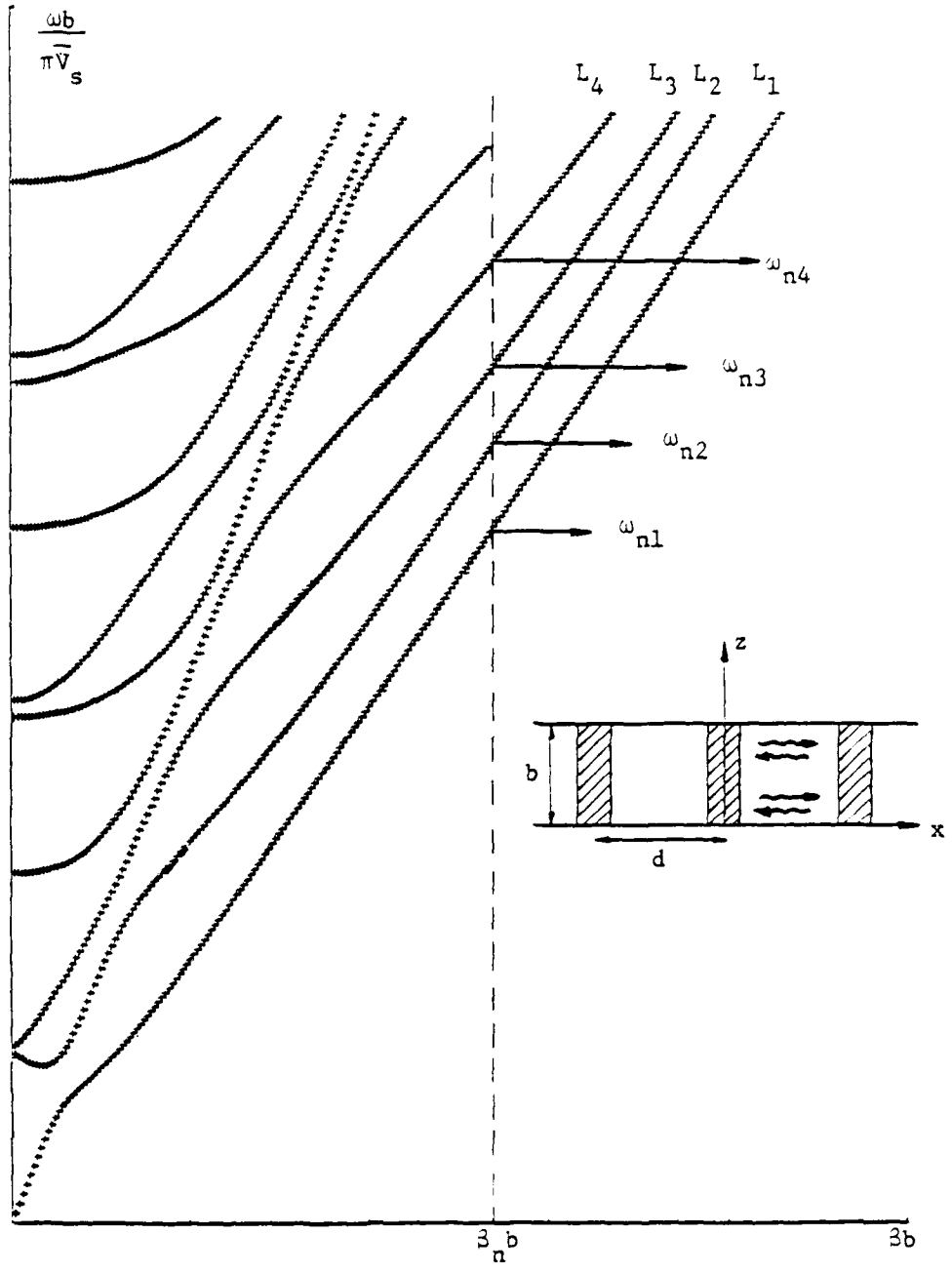

FIGURE 4

Definition of frequencies $\omega_{n\nu}$ in Eq. 4 of Appendix B, for the family of symmetric Lamb waves.

An additional feature of the Lamb wave formulation is that it leads to the average compliance (constant stress) material description of Eq. (2), rather than the average stiffness (constant strain) description of Eq. (1). It therefore more accurately represents the lateral resonances in a composite plate. This point is confirmed by the comparison of theory and experiment in subsection II.B. below.

B. Experiment

Comparisons of theory and experiment have been made using resonance spectra of the electric input impedance (Fig. 2) and laser probe measurements of elastic resonance vibration patterns over a unit cell of the composite. The second class of measurements has proved to be a powerful tool for positively identifying and classifying resonances. For reasons mentioned in subsection II.A, only the resonances f_ℓ, f_{t1} and f_{t2} of Fig. 2b are strongly excited in a uniformly electroded sample, and comparisons are made for only these resonances.

Many laser probe measurements have been performed, but only one example will be given here (Fig. 5). The figure shows recorded amplitude and phase of the vibration amplitude measured along a path between the rods in Fig. 3. Experimentally observed amplitude maxima in Fig. 5 are seen to occur at the zero position and at point *b* of Fig. 3. In Fig. 3(a), superposition of the *x*- and *y*-directed standing waves predicts a zero at the zero position and a maximum at point *b*; In Fig. 3(b), superposition of the two standing waves predicts maximum amplitudes at both the zero position and at point *b*. The latter behavior is in agreement with the experimental result in Fig. 5. It can also be seen by superposing the two standing waves in Fig. 3(b) that the vibration maximum at the zero position and that at point *b* are 180° out of phase, again in agreement with the experiment of Fig. 5. This comparison clearly identifies the motion as belonging to the diagonal resonance of part (b) in Fig. 3. Corroboration is provided by measurements taken at points *a*, *c* and *d* in Fig. 3, which were also found to be consistent with the superposed standing wave patterns in Fig. 3(b).

The above laser probe technique was used at Sanford to identify the vibration patterns of the resonances observed in certain selected samples among those listed in Table I. For these particular samples, the resonance spectra (as in Fig. 2(a)) measured at both Stanford and Penn State were found to be in close agreement. Most of the sample frequencies listed in Table I were measured at Penn State only,[1] and the resonant mode identification was made by comparison with samples that were laser-probed.

In Table I the piezoelectric rods are of PZT-5A and the polymer of Spurrs epoxy. Material parameters used in comparing theory and experiment are $\rho = 7.75 \times 10^3$ Kg/m^3, $V_\ell = 4032$ m/s, $V_s = 2263$ m/s for PZT-5A, and $\rho = 1.14 \times 10^3$ Kg/m^3, $V_\ell = 2207$ m/s, $V_s = 1003$ m/s for Spurrs epoxy. The parameters for PZT-5A were obtained from the

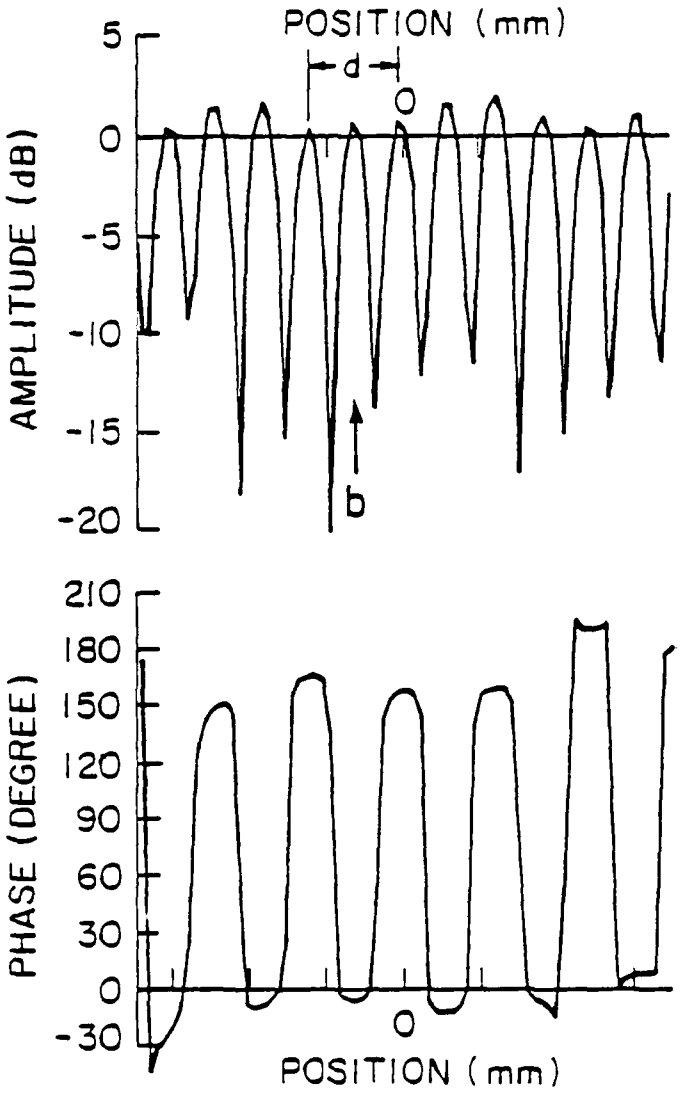

FIGURE 5

Laser scan measurement of acoustic displacement at f_{t2}, scanned between the rods (Fig. 3(b)).

TABLE I

Resonant Modes for PZT Rod-Polymer Composites*
(The numbers on the left correspond to the points plotted in Figs. 6–11)

Label of Plotted Point	Sample Number	v_c PZT	Thickness b (mm)	Spacing d (mm)	f_1 (anti-resonance) (KHZ)	f_2 (resonance) (KHZ)	f_3 (resonance) (KHZ)	Frequency Plotted
1	128**	10%	1.9	1.27	-	804	1096	f_2
2	2	5%	2.59	1.58	-	604	786	f_2
3	128**	10%	1.9	1.27	-	804	1096	f_3
4	10	5%	4.0	1.76	321.6	485	691	f_2
5	2	5%	2.59	1.58	-	604	786	f_3
6	11	5%	4.8	1.75	275.6	449	-	f_2
7	223	20%	2.54	0.90	612	894	-	f_2
8	122**	10%	3.64	1.27	-	662	1006	f_2
9	222	20%	3.05	0.90	519	830	-	f_2
10	12	5%	5.9	1.76	231.8	437	730	f_2
11	10	5%	4.0	1.76	321.6	485	691	f_3
12	130**	10%	5.15	1.27	296	644	-	f_2
13	228	20%	3.95	0.90	408	828	-	f_2
14	122**	10%	3.64	1.27	-	622	1006	f_3
15	12	5%	5.9	1.76	231.8	437	730	f_3
16	227	20%	4.60	0.90	353	886	-	f_2
17	226	20%	5.15	0.90	309	825	-	f_2
18	10	5%	4.0	1.76	321.6	485	691	f_1
19	11	5%	4.8	1.75	275.6	449	-	f_1
20	12	5%	5.9	1.76	231.8	437	730	f_1
21	130**	10%	5.15	1.27	296	644	-	f_1
22	227	20%	4.60	0.90	353	886	-	f_1
23	223	20%	2.54	0.90	612	894	-	f_1
24	228	20%	3.95	0.90	408	828	-	f_1
25	222	20%	3.05	0.90	519	830	-	f_1
26	226**	20%	5.15	0.90	309	825	-	f_1

*Measurements by T.R. Gururaja, Materials Research Laboratory, The Pennsylvania State University.

**Sample also tested at Stanford University.

manufacturer's data, using piezoelastically-stiffened elastic constants and assuming isotropy. Spurrs epoxy parameters were measured at Stanford, using pulse echo methods to determine the velocities. Frequencies listed in the table are the anti-resonance frequencies for the longitudinal thickness mode (f_1) and the resonance frequencies for the lateral modes (f_2, f_3). In Fig. 2(a), the resonance frequencies are points of impedance minimum and the anti-resonance frequencies are points of impedance maximum. A resonance frequency corresponds approximately to the *short-circuit* natural frequency of the freely vibrating piezoelectric resonator mode, and an anti-resonance frequency to the *open-circuit* natural frequency of the free resonator mode. Since our composite theory does not yet include piezoelectricity, the choice of which experimental frequency to compare with theory is not immediately obvious. Our choice was based on the following considerations: (1) In the Mason model for a parallel plate transducer/resonator, the open circuit (or anti-resonance) frequencies correspond to pure $n\lambda/2$ standing waves across the plate;[6] for this reason, the anti-resonance frequencies are chosen to compare with the theory of the longitundinal thickness resonance ($f_1 \equiv f_t$). (2) For the lateral resonances (f_2, f_3), the standing waves are parallel to the electrode faces (Fig. 2(b)) and the choice between resonance and anti-resonance frequencies is not clear at this point; consequently, the resonance frequencies were chosen simply because they give a better fit to the theory.

In subsection II.A above, it was noted that the constant strain model of Appendix A is more appropriate for calculating the longitudinal thickness resonances, while the constant stress model of Appendix B is more appropriate for the lateral resonances. Figures 6–11 compare theory and experiment for these two cases. Figures 6–8 represent the dispersion curves for the symmetric Lamb modes * calculated from spatially averaged stiffnesses (the constant strain model). On these curves the frequencies of the longitudinal thickness resonances for samples in Table I are plotted at $\beta b = 0$. They lie very close to the $\beta b = 0$ intercept of the second symmetric Lamb mode, a point that correponds to the longitudinal thickness resonance in a homogeneous plate. Plots of lateral resonance frequencies (at $\beta = 2\pi/d$, corresponding to the resonance conditions in Fig. 2(b)), lie far below the Lamb waves spectrum in Figs. 6–8. This is unreasonable physically because the lateral resonances correspond to Lamb waves that are Bragg scattered by planes of piezoelectric rods; and these points are therefore not shown.

In Figs. 9–11, the curves are Lamb wave spectra calculated from spatially-averaged compliances (i.e., the constant stress model). The experimental longitudinal thickness resonances (f_1) are now seen to be in poor agreement with the theory, but the lateral resonances (f_2, f_3) (plotted at $\beta = 2\pi/d$) lie close to the lower modes of the symmetric Lamb spectrum, as expected from Appendix B. The experimental points are distributed along the dispersion-curves

*Antisymmetric modes cannot be excited in plates driven by PZT rods poled normal to the plane of the plate.

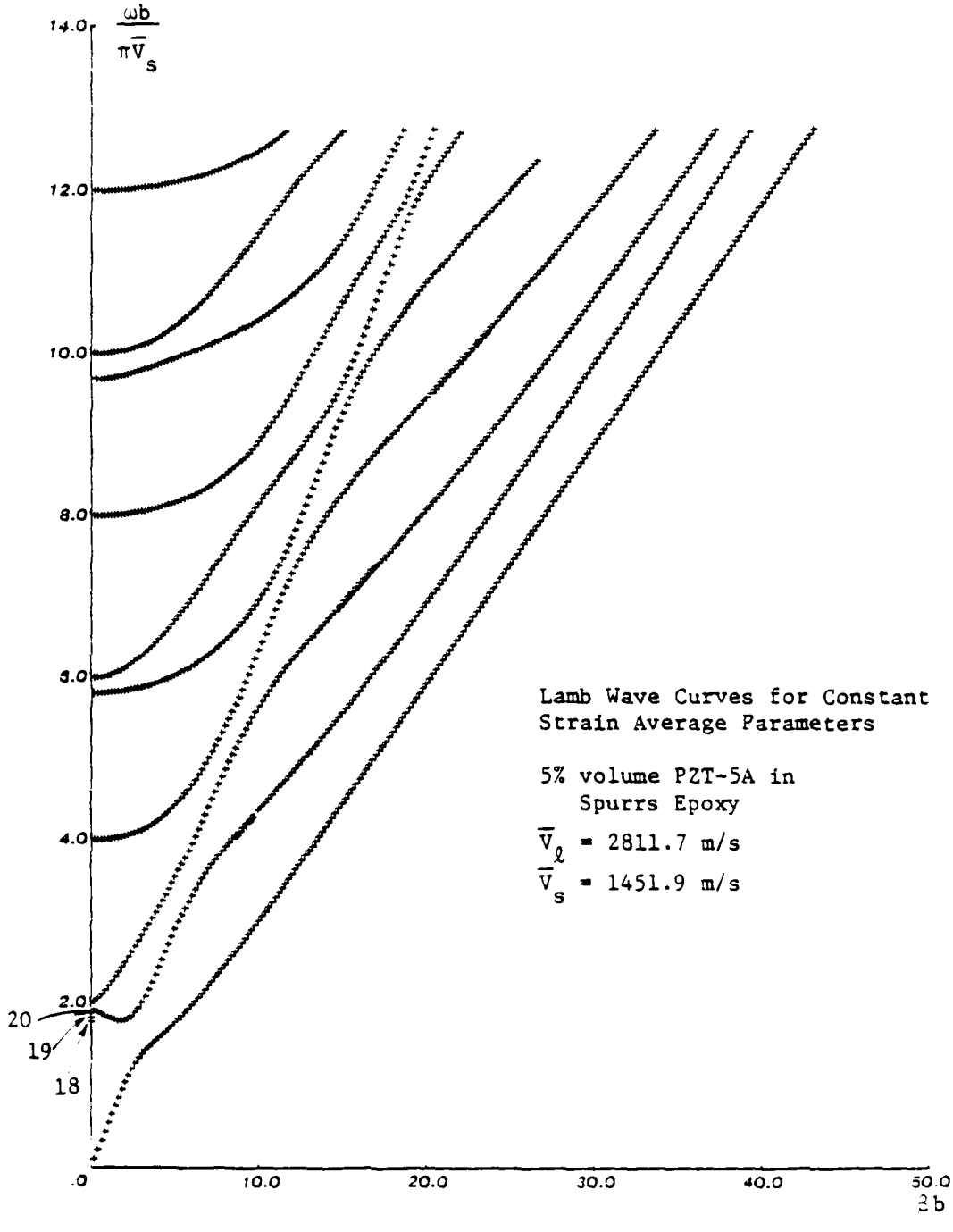

FIGURE 6

Comparison of constant strain model with experiment (5% volume ratio).

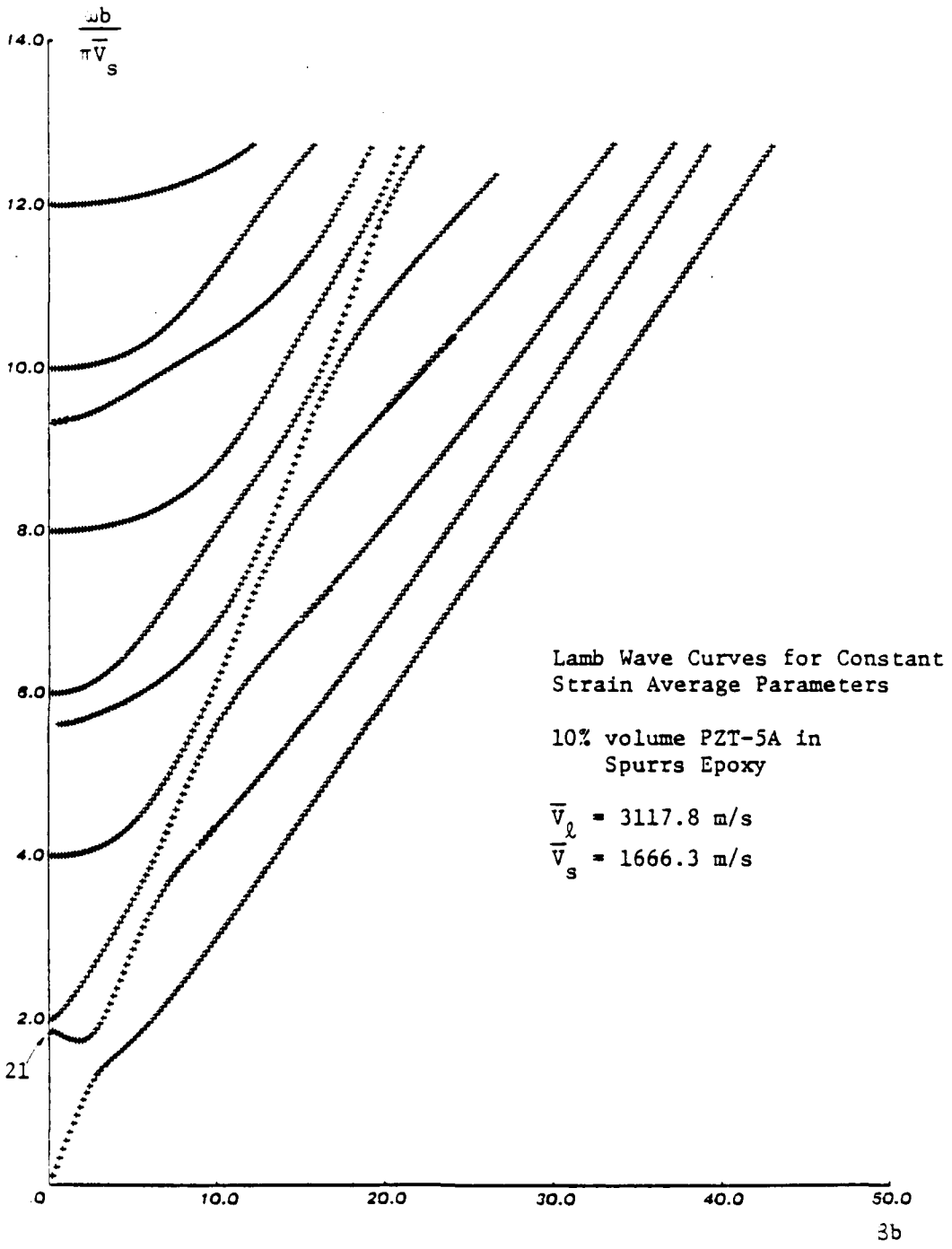

FIGURE 7

Same as Fig. 6 (10% volume ratio).

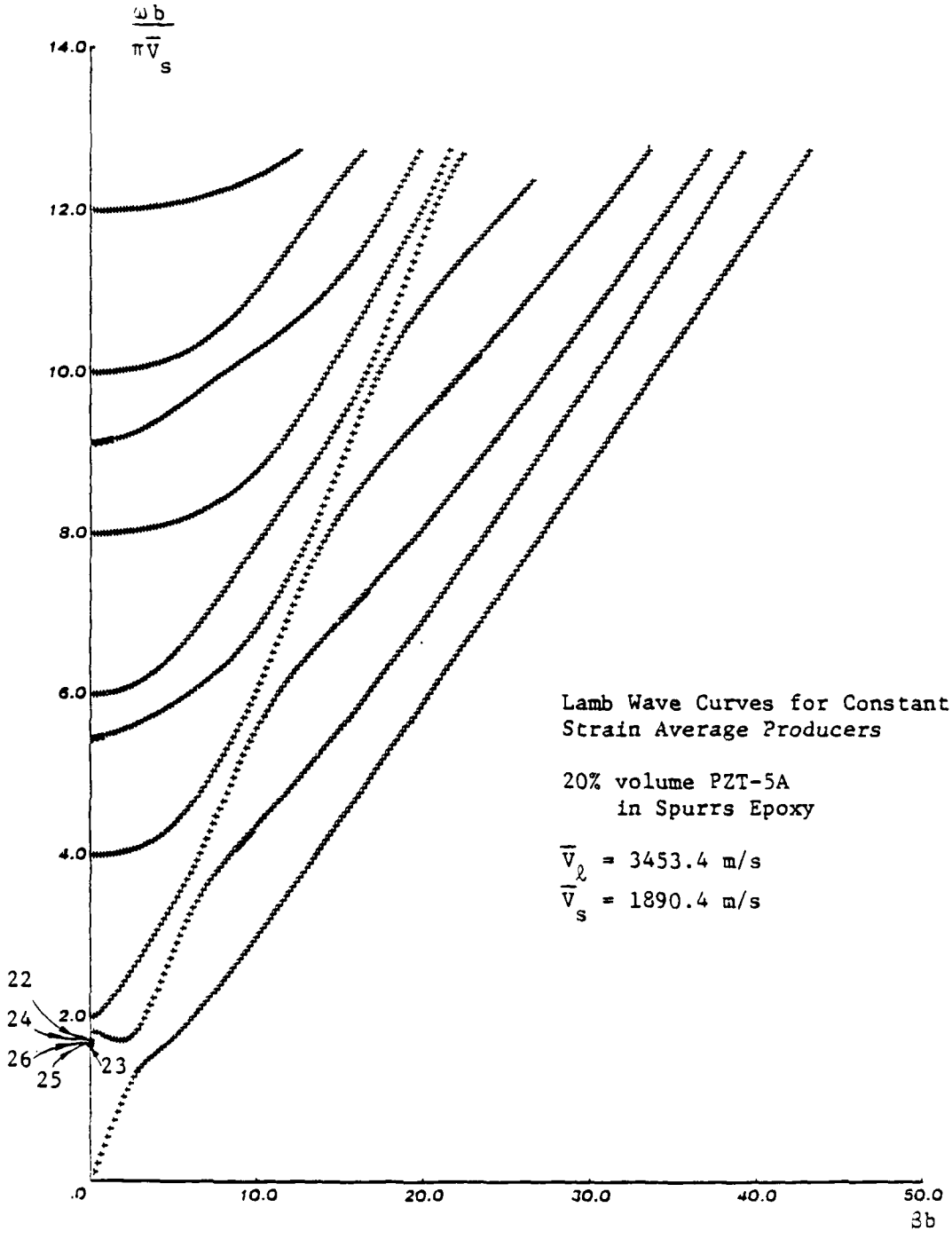

FIGURE 8

Same as Fig. 6 (20% volume ratio).

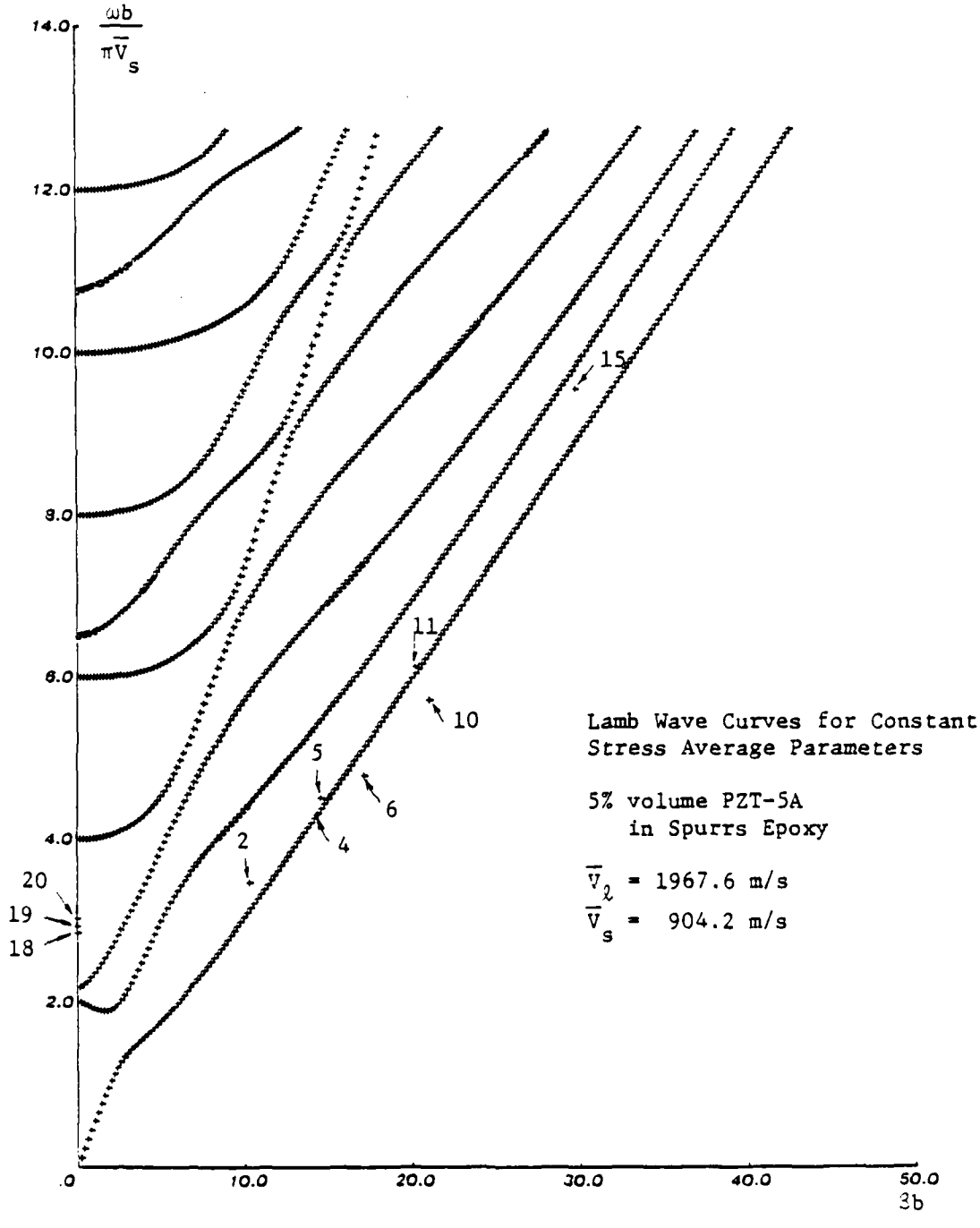

FIGURE 9

Comparison of constant stress model with experiment (5% volume ratio).

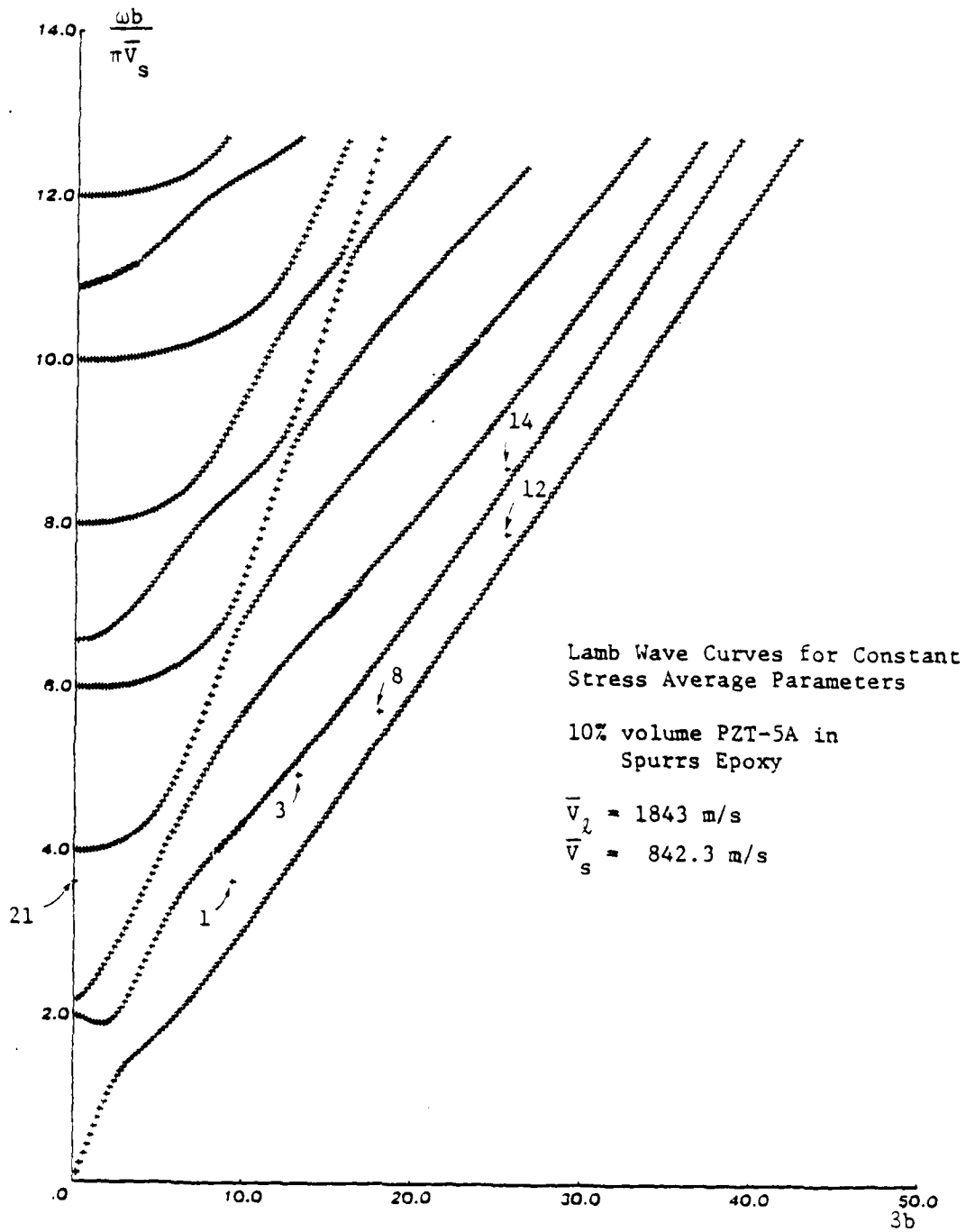

FIGURE 10

Same as Fig. 9 (10% volume ratio).

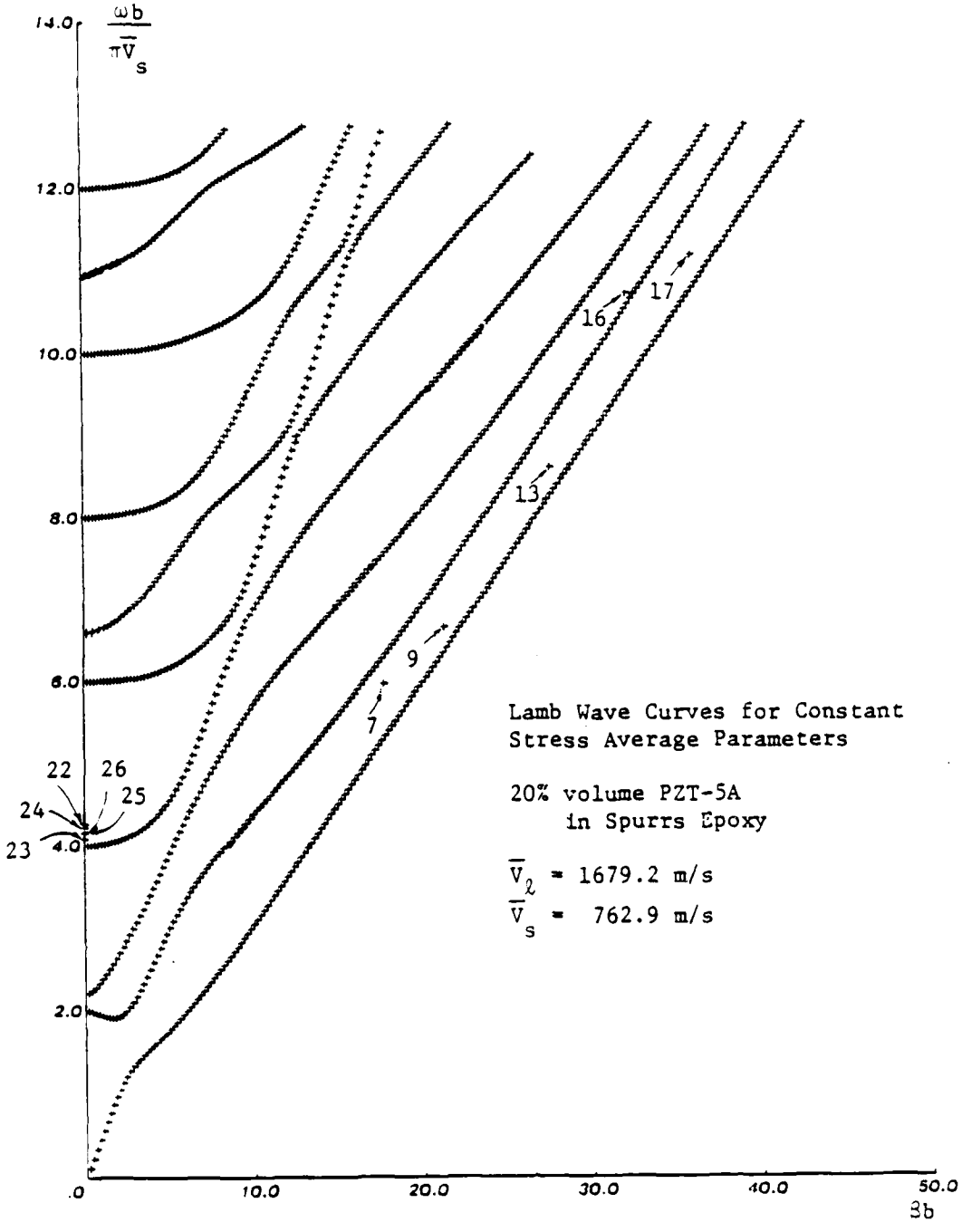

FIGURE 11

Same as Fig. 9 (20% volume ratio).

and trace out the Lamb wave dispersion curves quite accurately.

C. Discussion

Experimental points plotted in Figs. 6–11 clearly show the expected behavior—i.e., longitudinal thickness resonances are best represented by the constant strain model and lateral resonances by the constant stress model, for volume percentages of PZT as large as 20%. In this comparison, the longitudinal thickness resonance is analysed by completely neglecting any coupling into other space harmonics, and the lateral resonances are analysed by the coupled mode approximation. These approximations are expected to be somewhat inaccurate, even in the 5% volume ratio case, and this fact may account for some of the disagreement observed in Figs. 6–11. Continuing analysis should add more and more space harmonics to the calculation until there is no further change in the result.

Another possible source of error is the incomplete treatment of piezoelectricity and anisotropy in the PZT. One important consequence of piezoelectric coupling was discussed in subsection II.B. with respect to the choice of the longitudinal thickness anti-resonance for comparison with theory. The theoretical basis for choosing to compare lateral mode experiments with theory on the basis of resonance frequencies has not yet been formulated. Another area of uncertainty is how best to characterize piezoelectric stiffening of the elastic constants in a composite medium.

Despite these unresolved questions, agreement of theory and experiment in Figs. 6–11 is quite sufficient to permit drawing practical conclusions and to explain and predict various aspects of the behavior of composites. In many experimental resonance curves a number of small supplementary resonances are observed above and below f_{t1} and f_{t2}. These can be explained by observing that Eq. (3) couples among all Lamb waves in all orders of space harmonic, and that additional couplings occur in the two-dimensional version of the equation. Bragg resonances therefore occur for the higher order Lamb modes, but are weakly excited by the electrodes.

Understanding the resulting structure of the dispersion curves is best reached by using the reduced zone scheme for the dispersion curves, as in the electronic theory of solids.[7] This can be visualized by referring to Fig. 4, and supposing that

$$\beta_n b = \frac{2\pi b}{d}, \tag{4}$$

which corresponds to the $d = \lambda$ stopbands discussed above. The reduced zone scheme is generated by folding the figure along the vertical line through $\beta_n b$, so that the parts of the curves on the right cross the parts of the curves on the left. Each crossing point corresponds to a Bragg-matching condition, where the crossed curves split into stopbands. Crossings on the vertical line through $\beta_n b = 2\pi b/d$ represent Bragg-scattering of a Lamb mode into

itself; these are the most strongly excited. Other crossings are for Bragg-scattering from one Lamb mode into another. At these points, the band edge resonances do not have piezoelectric rods vibrating in phase, so that they are less strongly excited than in the first class of band edge resonances. Even in this one-dimensionally periodic model, there exists a large density of stopbands in the frequency range above the lowest stopband frequency; and in a two-dimensionally periodic structure this density is further increased by the proliferation of two-dimensional Brillouin zones. Such features will be extremely important in determining the scattering behavior of periodic composite materials, and may even be applicable in designing and fabricating anti-reflection layers.

The discussion in the paragraph above is also relevant to the behavior of observed resonance spectra curves as a function of the ratio of b/d in Fig. 4. Since the curves are normalized to b, setting $\beta_n = 2\pi/d$ places the vertical dashed line at a position that moves to the left as d increases. This means that the position of the lowest lateral stopband resonance moves steadily to the left with increasing d, as can be tracked by comparing the points plotted in Figs. 9–11 with their listed composite dimensions in Table I. Eventually, as d increases, the lowest stopband frequency approaches coincidence with longitudinal thickness resonant frequency (at the $\beta_n b = 0$ intercept of the second Lamb mode in Figs. 6–8, since the constant strain model must be used for this resonance). This phenomenon has been observed in experiments at Penn State, and an apparent coupling of the thickness and lateral modes has been found to occur as their frequencies cross. Practically, the most important impact of this Lamb mode Floquet theory is in providing a physical basis for optimally choosing the ratio b/d in transducer and resonator design. However, explaining the mode coupling phenomenon observed at Penn State may also turn out to have significant practical consequences.

III. PMN-BASED TRANSDUCERS

The goal of the research is to study acoustic wave propagation in ceramic materials in which spatially varying polarization patterns are established, with the aim of exploring novel signal processing technology and applications. Initial work will be conducted with lead magnesium niobate (PMN) and lanthanum modified lead-zirconate lead-titanate (PLZT) ceramics. These materials exhibit a strain which is proportional to the square of an externally applied electric field, i.e., electrostriction. In addition, suitable compositions do not possess remanent polarizations. It is this latter property that may be most interesting for certain device applications, since it permits rapid switching of transducer configurations.

Three experiments are currently being planned. The first is a basic study of some electro-mechanical properties of the above-mentioned ceramic materials. Since these materials do not possess a remanent polarization, the electro-mechanical parameters are a function of an externally applied biasing field. This first experiment will measure this dependence using a plate transducer structure of thickness t and area W by L. The parallel plate structure was chosen so that the externally applied field could be determined from readily measured factors (in this case the externally applied voltage and the thickness of the wafer). The basic electrical measuring circuit is shown in Fig. 12. It is an impedance measuring system.

The second experiment uses the structure shown in Fig. 13(a). It is intended for use as a surface acoustic wave (SAW) device. The idea for this structure is based upon other SAW devices using piezoelectric materials that can be modeled as possessing the hexagonal type of symmetry. In those devices, the material is oriented so that the c-axis is perpendicular to the major face containing the surface electrodes. For ceramics, the "c-axis" will be colinear with the electric field. Thus, in our case, a DC bias field will be established between the full surface electrode on one surface and the electrode pattern on the opposite surface. The relationship between the various dimensional parameters is governed by two factors: acoustics and electrostatics. Electrostatic considerations lead to the following relations:

$$(w+g)/t << 1 \qquad w/g > 1 \tag{5}$$

Basically, these relations insure that the configuration produces an electrostatic field which approaches the ideal parallel plate field. One practical consideration is that, from an operating voltage point of view, we do not want t to become too large. Acoustic properties lead to the following relations:

$$(w+g)/t << 1 \qquad w/g = 1 \tag{6}$$

Clearly, the first relation is desirable since we want pure surface waves, which require that the second surface be very far from the top surface.

Finally, we need to study the effect of the fringing fields near the electrode edges. We intend two methods for this study. The first is to develop a computer program to solve

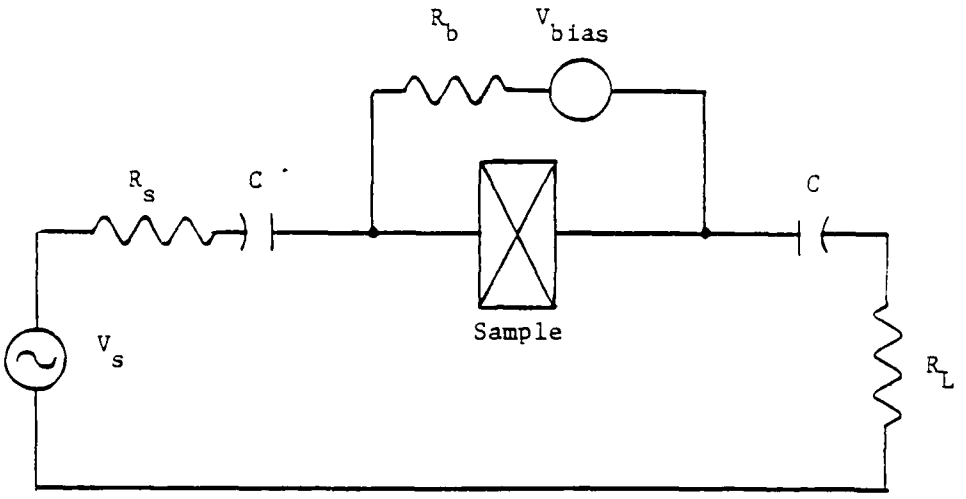

FIGURE 12

PMN impedance measuring circuit.

the electrostatic field problem, and the second is to experimentally measure the field. This second method will use the PLZT material. This ceramic material is optically active, i.e., it is uniaxially birefringent. Since the dielectric properties of both ceramics are very similar, the fields obtained for the PLZT device will be directly applicable to the PMN device. The structure intended for this experiment is shown in Fig. 13(b).

We plan to use two different polarizer configurations: a circular polarizer and a linear polarizer. With the circular polarizer configuration we can measure the magnitude of the electric field irrespective of its direction. Then, using the linear polarizer, we can measure the orientation of the field. Thus, with this approach, the computer-generated solution can be checked and confidence built for its use in other configurations.

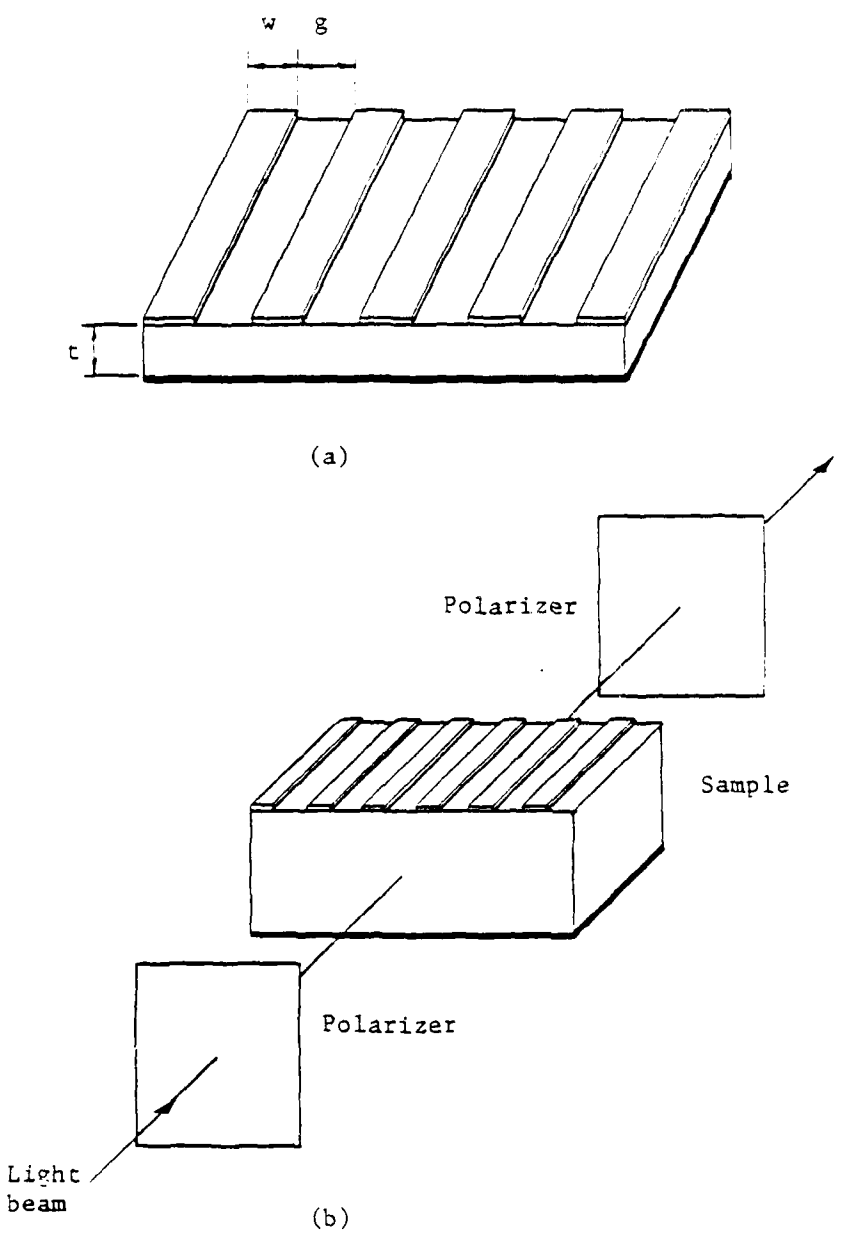

FIGURE 13

PMN biased SAW transducers: (a) Schematic; (b) Optical configuration for observing electric field distribution.

IV. INTERFACE WAVES

Ferroelectric ceramics poled with a pattern of spatially varying remanent electric polarization have been employed in a number of novel device applications. These range from optical displays and memories in transparent piezoceramics to Fresnel-type focusing transducers for ultrasonic imaging in medicine and nondestructive evaluation. For these devices, a uniformly poled piece of ceramic is reverse-poled in certain regions to effect a desired spatial pattern of reversed piezoelectric coupling. Transition zones separating regions of unlike remanent polarization, analogous to domain walls in ferroelectric crystals, arise as a consequence of this regional counter-poling process. While the transition from one polarization state to another in a single crystal is quite abrupt (domain wall thicknesses less than a lattice constant are typical), the transition in a differentially-poled ceramic is comparatively gradual. It has been shown theoretically and experimentally that both abrupt and gradual polarization transition zones are capable of supporting guided acoustic waves.[8] Abrupt transitions were realized by glueing together two uniformly polarized ceramic plates along an edge, with the two polarizations reversed. Gradual transition zones are fabricated by depositing electrode patterns on an already poled ferroelectric ceramic and counter-poling under the electrodes.[8] This creates waveguiding polarization transition zones around the edges of the electrodes, in spatial patterns determined by the electrode geometries.

In this way, single mode acoustic waveguides can be fabricated in ferroelectric ceramic wafers, using simple inexpensive differential poling techniques. "Acoustostrip" waveguide components based on this concept may be conceived in all of the microstrip waveguide geometries utilized in microwave integrated circuit technology—i.e., parallel line directional couplers, ring resonators, hybrids, channel-dropping filters, etc. Directional coupling action has been already demonstrated experimentally—first, at 1 MHz[9] and, more recently, at several megaherz. The significance of this new technology is that it has potential for realizing integrated acoustostrip filters and signal processing systems (operating up to, perhaps, 10 MHz) on a single ferroelectric wafer. A possibility also exists for creating, on *single crystal* wafers, poled-in systems of this kind for operation at frequencies up to hundreds of megaherz. Materials such as PMN (section III, above) may eventually be developed in sufficiently high quality to permit realization of switchable acoustostrip waveguide systems controlled by an electric bias field.

A. Waveguide Fabrication and Characterization

In poling an acoustostrip waveguide duct into an initially uniformly poled ferroelectric ceramic wafer, a variety of electrode structures may be used. For a single duct, the electrode covers the entire half of the wafer on one side of the duct; for a pair of ducts, a strip electrode is used (Fig. 14 (top)). In either case a waveguide duct is centered on each zero

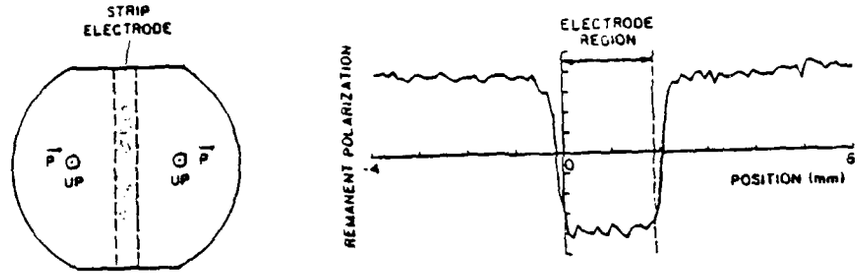

(1) FABRICATION PROCEDURE

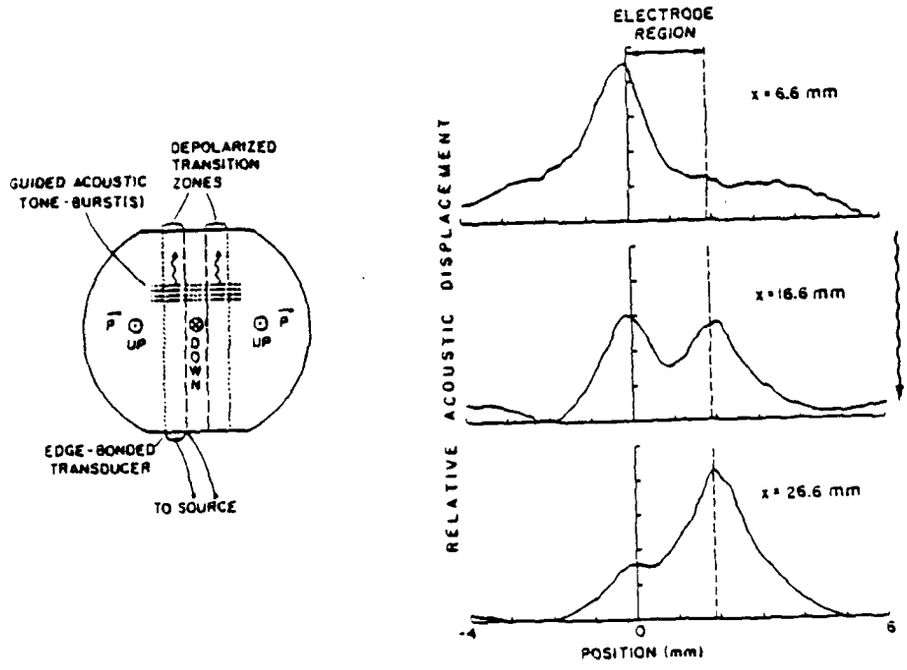

(2) DIRECTIONAL COUPLER

FIGURE 14

Acoustostrip waveguide processing on a ferroelectric wafer.

crossing of the polarization profile. The experimental curve at the top right of Fig. 14 shows a profile creating two such ducts, spaced approximately by the width of the strip electrode. (Experimental procedures and instrumentation are dicussed in section IV.C below). Another electrode configuration, with tapered ends suitable for directional coupler fabrication, is shown in Fig. 15.

Parameters important in the fabrication of these waveguides are: (1) properties of the ferroelectric ceramic, (2) thickness of the wafer, and (3) curvature of the electrode edges. The properties of the ceramic play a fundamental role in establishing the width of the waveguide duct, which is related to the slope of the polarization transition profile (Fig. 14, top right). This width is important because it determines whether or not the waveguide propagation is single mode or multimode. Experiments have been performed on both a hard ceramic (PZT-4) and a soft ceramic (PZT-5H),[8] showing that PZT-4 produced narrow ducts (singlemode) and PZT-5H broad ducts (multimode).

A conflicting requirement on the choice of ceramic is that it must have as large a Q as possible at megaherz frequencies. There exists, at present, essentially no qualititative data in the ferroelectric ceramics literature concerning Q as a function of frequency. However, our waveguide experiments show that PZT-5H (in which single mode waveguides were easily realized) has unacceptably large attenuation losses. A compromise candidate has been found in PZT-8. This is a hard ceramic with good high frequency Q, but it also generates counter-poled ducts of widths only slightly broader than those in PZT-5H. The exact physical phenomenon determining the duct width.as not yet been identified; but in the materials listed a correlat' n has been noted between large elastic stiffness and broad duct width. Barium titanite ceramics should also be studied in the future, to further explore this question.

Finally, the thickness of the ceramic wafer and the curvature of the electrode edge influence the width of the electrode fringing field, and therefore also control the width of the region subject to depoling. (Figure 16 illustrates a calculated plot of the fringing field near the edge of a depoling electrode on ceramic). The width of the fringing field region decreases with the thickness of the wafer; and it has been confirmed experimentally that duct widths are narrower on thinner wafers. This is another factor to be considered in designing these acoustostrip waveguide structures.

Measurements of guided wave propagation were reported on both PZT-4 and PZT-5H single acoustostrip waveguides in Reference 8. These experiments were performed using a new method of wave excitation (edge bonded transducers) that has turned out to be a superior method for creating clean, localized acoustic excitation profiles. Laser probe measurements were made in the pulse mode to determine the amplitude profile of the propagating duct wave. Very accurate propagation velocity measurements were also carried out, and these gave glue-bond *and* transition wave velocities in very good agreement with theoretical predictions.

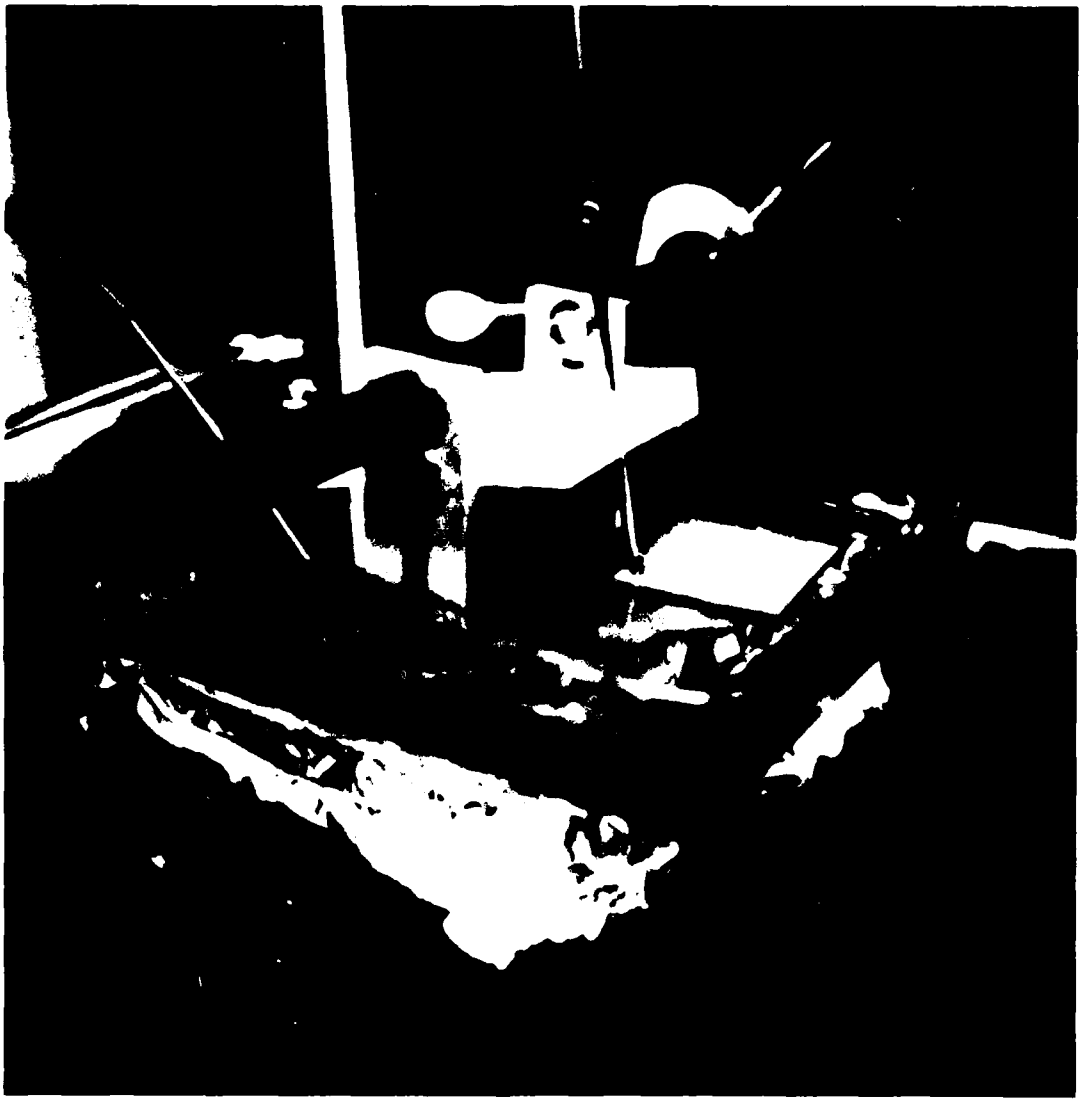

FIGURE 15

Differential poling apparatus

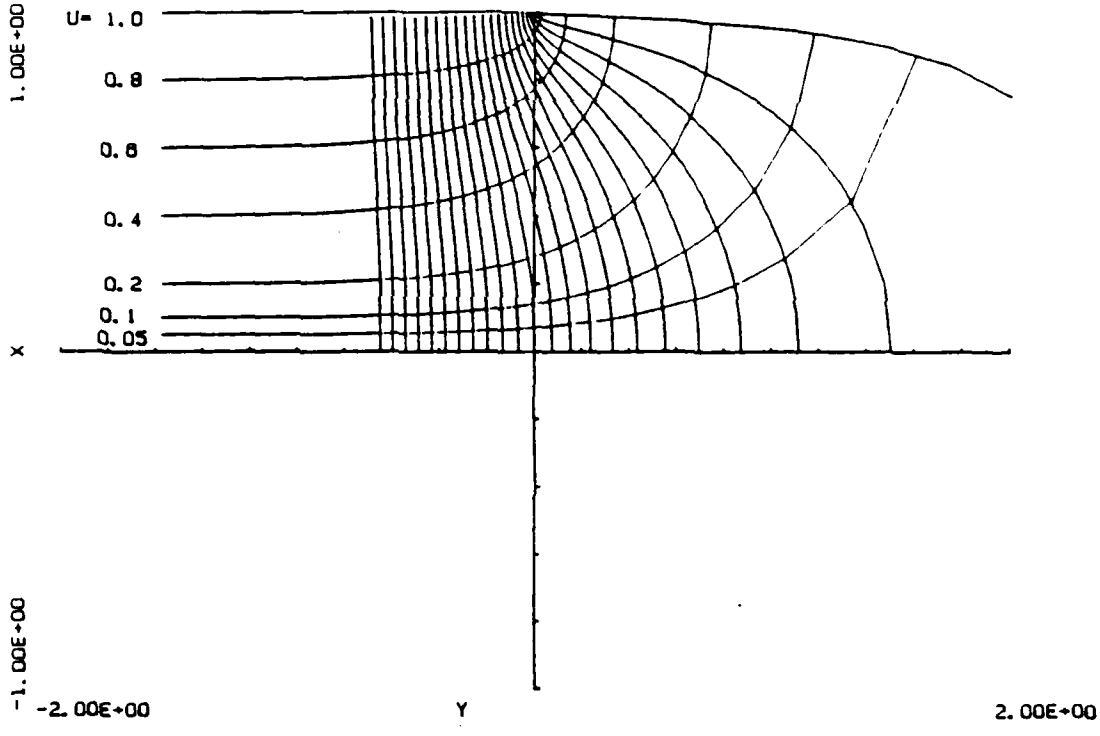

FIGURE 16

Calculation of fringing fields outside poling electrodes.

Improper poling conditions and/or inferior ceramic may result in cracking within the poling transition zone. Interface waves scatter strongly from such flaws and provide an excellent means for probing the integrity of transition zone structures intended for waveguide or other applications.

B. Directional Couplers

The bottom part of Fig. 14 shows our first acoustostrip waveguide structure designed to test the directional coupling principle.[9] Two closely-spaced waveguide ducts were created in the depolarized transition zones at the edges of a strip electrode (Fig. 14, top). Coupling between the waveguides is adjusted by controlling the electrode width, so that the two guided wave profiles overlap. In the light of the discussion in section IV.A above, it can be seen that this overlap will also be affected by the properties of the ceramic and by the wafer thickness. Directional coupling action was demonstrated by laser probing the acoustic vibration amplitudes on the two parallel acoustostrip guides. An example of measured data is shown at the lower right of Fig. 14, where the wave is launched at the top of the set of curves and proceeds downward. It is seen that transfer to the second guide occurs after a travel distance of 26.6 mm. This data was taken using 8-cycle tonebursts at 1 MHz on a PZT-5H plate 3.81 mm thick and with a diameter of approximately 51 mm. As described in Reference 9, the effective spacing of the coupled waveguides was subsequently decreased by applying a reversed depoling voltage (6.3 KV/cm) to the electrode for 60 seconds. The effect of this was to increase the coupling and to decrease the energy transfer distance from 26.6 mm to approximately 11.6 mm. Voltage control of directional coupling could be very significant in PMN structures, if waveguide fabrication should prove to be practical in these materials.

A new generation of acoustostrip directional couplers has now been fabricated, with tapered duct spacing at the input and output to provide better isolation. Figure 15 shows one of these devices in the poling station, where the tapered depoling electrode is clearly visible. In Fig. 17, the processed device is shown with the poling electrode still in place; and in Fig. 18 it is shown mounted in the text fixture, with the electrode removed. These devices are being tested in the pulse mode at frequencies up to 7 MHz. The objectives are to carefully quantify the S-parameters of the devices and to obtain quantitative data relating performance to the fabrication parameters (i.e., poling profile shape, wafer thickness, and material properties). This will lead to better physical understanding of how the polarization response of the ceramic can be tailored to suit various eventual device applications (directional couplers, resonators, filters, etc.).

C. Instrumentation

To obtain the above results and to prepare for achieving the device characterization goals

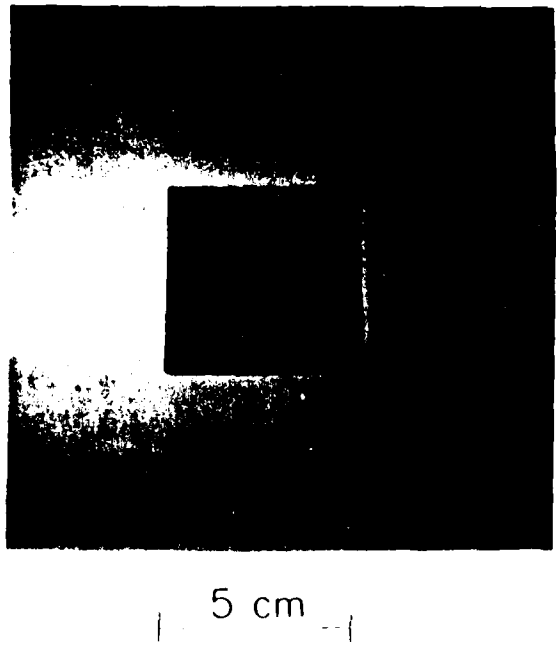

FIGURE 17

PZT-5H wafer with poling electrodes still in place.

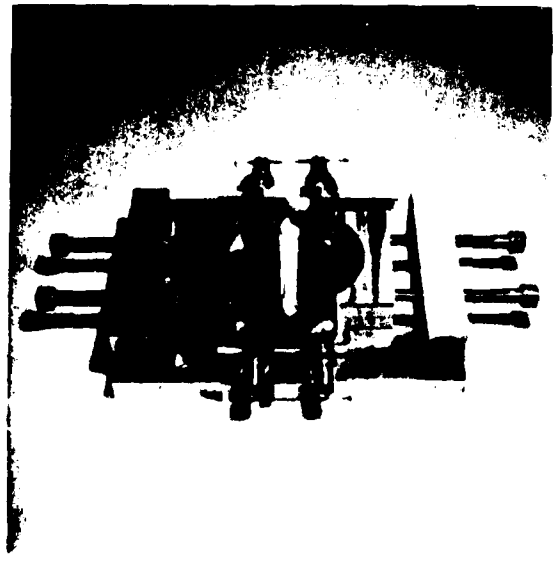

FIGURE 18

PZT-5H directional coupler in test fixture. Poling electrodes have been removed.

stated at the end of section IV.B, it has been found necessary to improve our laser probe and poling system.

Laser Probe. During the current reporting period, the laser probe was interfaced with a dedicated laboratory microcomputer. Software was written and hardware developed to control the sample scanning mechanisms fully automatically, and to acquire and plot data. (This facility has also played an essential part in the composite material studies of section I). The electronics of the laser probe detection system has been modified to permit measurement of acoustic tone bursts at carrier frequencies up to 7 MHz.

Poling Apparatus. To permit rapid characterization of the poling conditions, new recording instrumentation has been developed. The circuit used is illustrated in the insert of Fig. 19, where the series resistor is intended to limit current flow in the event of breakdown, and the current integrator monitors the degree of poling achieved under various conditions. During a poling operation, the amount of charge flowing through the integrator is

$$\begin{aligned} \Delta Q_{total} &= \Delta Q_{initial\,charge} + A(\Delta P) - \Delta Q_{discharge} \\ &= A(\Delta P), \end{aligned} \tag{7}$$

where A is the electrode area and ΔP is the change in ceramic polarization due to poling. Figure 19 illustrates data taken in this way for a PZT-5H sample, with the process allowed to run to completion at each value of poling field. The same system can be used to quantify poling conditions as a function of time.

V. SUMMARY OF SIGNIFICANT ACOMPLISHMENTS

(1) Floquet theory of periodic composite plates developed and compared satisfactorily with frequency resonance spectra measured at Penn State on a large variety of samples. This theory predicts dependence of the lateral resonance frequencies on the thickness/spacing ratio for the PZT rods in plastic plates, with percentage volume rates up to 20%.

(2) Characterized the dependence of interface waveguide duct thickness (acoustostrip waveguide) on the material properties of the ceramic and on the plate thickness.

(3) Experimental demonstration of acoustostrip directional coupler action at frequencies up to 7 MHz.

(4) Extended the operation of the laser probe up to 7 MHz in the pulsed mode.

(5) Developed new circuitry for rapidly monitoring the poling state in fabricating differentially poled samples.

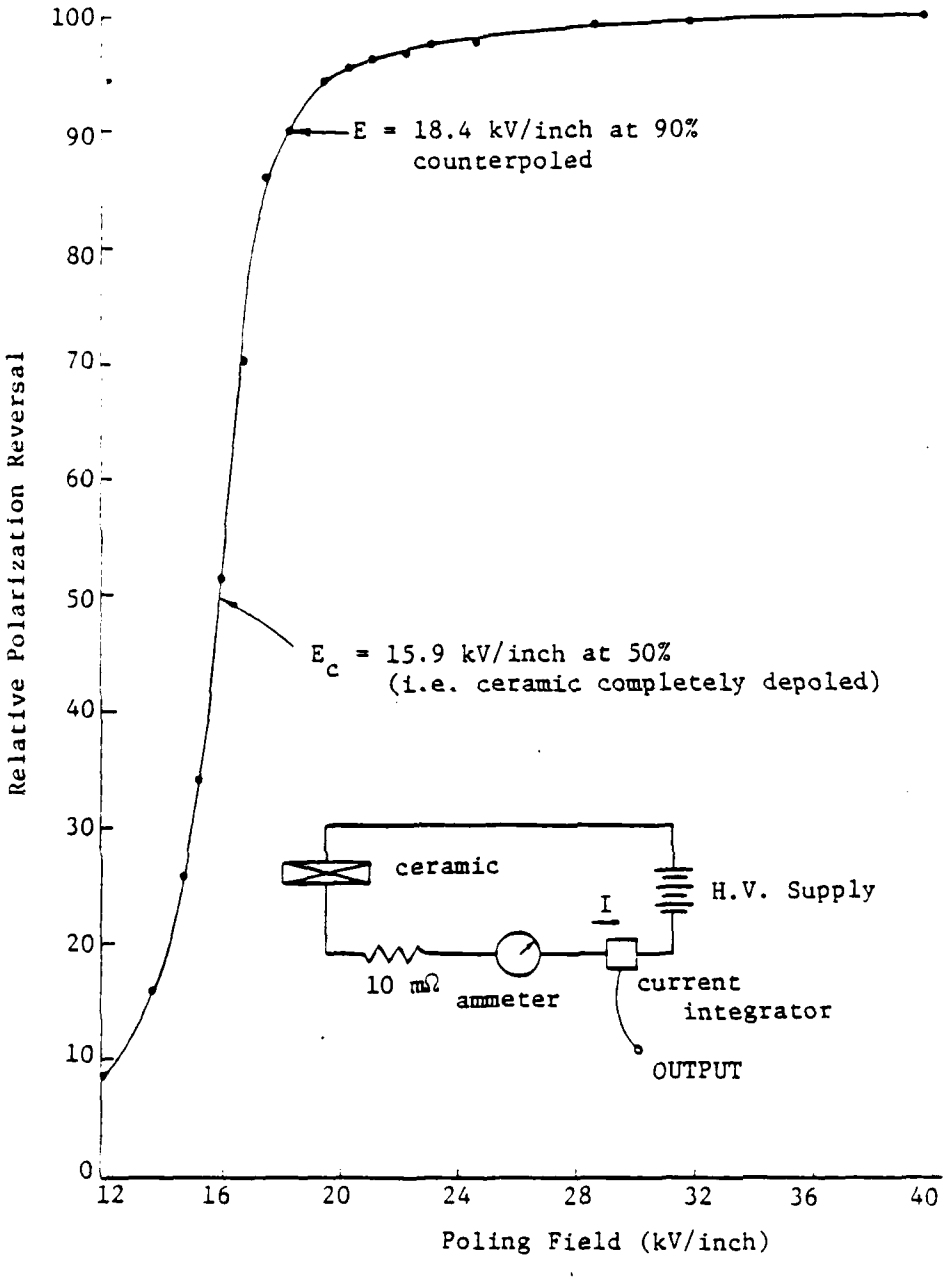

FIGURE 19

Relative polarization versus poling field measurements (PZT-5H at room temperature).

VI. REFERENCES

1. T.R. Gururaja, W.L. Schulze, L.E. Cross, B.A. Auld, Y.A. Shui, and Y. Wang, "Resonant Modes of Vibration in Piezoelectric Composites with Two Dimensional Periodicity," presented at the 5th European Meeting on Ferroelectricity, Benalmadena (Malaga), Spain, September 1983 (*Ferroelectrics* **54**, pp. 183–186 (1983)).
2. B.A. Auld, Y. Shui, and Y. Wang, "Elastic Wave Propagation in Three-Dimensional Periodic Composite Materials," presented at the International Conference on the Dynamics of Interfaces, Lille, France, September 1983 (to be published in *Journal de Physique*).
3. B.A. Auld, H.A. Kunkel, Y.A. Shui, and Y. Wang, "Dynamic Behavior of Periodic Piezoelectric Composites," *Proc. 1983 IEEE Ultrasonics Symposium* (Catalog No. 83CH1947), 554–558 (1984).
4. S. Ikegami, I. Ueda and S. Kobayashi, "Frequency Spectra of Resonant Vibration in Disk Plates of $PbTiO_3$ Piezoelectric Ceramics," *J. Acous. Soc. Am.* **55**, 339–344 (1974).
5. B.A. Auld, *Acoustic Fields and Waves in Solids*, Vol. II, Chapter 11 (New York: Wiley-Interscience, 1973).
6. B.A. Auld, *Acoustic Fields and Waves in Solids*, Vol. I, p. 324–327 (New York: Wiley-Interscience, 1984).
7. J.M. Ziman, *Principles of the Theory of Solids*, p. 23 and pp. 72–73 (Cambridge: University Press, 1964).
8. H.A. Kunkel and B.A. Auld, "The Use of Guided Acoustic Interface Waves in the Study of Differentially Poled Piezoelectric Ceramics," presented at the 1983 IEEE International Symposium on APPLICATIONS OF FERROELECTRICS (ISAF), Gaithersburg, Md., May 1983 (*Ferroelectrics* **51**, 99–104 (1983)).
9. H.A. Kunkel and B.A. Auld, "Acoustic Interface Waveguide Directional Coupler," *Proc. 1983 IEEE Ultrasonics Symposium* (Catalog No. 83CH1947), 562–565 (1984).

VII. APPENDIX A

From *Proceedings of Ultrasonics Symposium*, 1983 (Reference 3)

DYNAMIC BEHAVIOR OF PERIODIC PIEZOELECTRIC COMPOSITES

B. A. Auld, H. A. Kunkel, Y. A. Shui,* and Y. Wang

Edward L. Ginzton Laboratory
Stanford University
Stanford, California 94305

Abstract

Composite piezoelectric transducer materials consisting of two- and three-dimensional periodic arrays of piezoelectric ceramic elements (i.e., rods, spheres, etc.) in a plastic matrix now play an important role in hydrophone technology. These materials were conceived and developed on the basis of strictly static elasticity considerations, suitable for general aspects of hydrophone performance, but in order to completely understand and exploit such materials it is essential to fully develop a theory of their dynamic behavior. This paper presents a general Floquet theory of wave propagation in periodic elastic composites and develops detailed results for composite plates consisting of ceramic rods imbedded in a plastic matrix. Laser probe measurements of the vibration distribution in such plates show good agreement with theory.

1. Introduction

The design and fabrication of artificial materials for special purposes is a rapidly growing technology, with applications spanning the range from mechanical structures to electronic devices. An important class of these new materials is the family of piezoelectric-polymer composite transducers for various sonic and ultrasonic devices.[1] In designing such materials, consideration is given to choosing the component phases of the composite material so as to maximize some figure of merit for the application envisaged. For example, in an electromechanical transducer one might want to maximize the piezoelectric coupling, minimize the density and optimize the acoustic match to water. Single phase materials, such as ceramic piezoelectrics and plastic piezoelectrics, are not themselves optimum in all these respects and the goal in composite material design is to find the best combination of phases. For example, it has been found that composites consisting of PZT rods imbedded in a plastic matrix have certain piezoelectric coupling coefficients that are much superior to those of homogeneous PZT.[1] Many different regular two-phase (PZT and plastic) composite structures (or lattices) have been fabricated and studied in the low frequency (long wavelength) regime, where the periodicity of the structure is small compared with the acoustic wavelength. This is appropriate to hydrophone applications. More recently interest has been directed toward the behavior of these materials in the frequency range where the structural period is comparable to a wavelength and where the material itself exhibits frequency-dependent behavior similar to that of vibrations of a crystal lattice near the Brillouin zone boundary. Quantitative understanding of this phenomenon is necessary for an evaluation of the role of these materials in transducer applications at higher frequencies.

2. Floquet Theory for Two-Dimensional Composites

Although the theory presented here is applicable to full three-dimensional lattices of arbitrary inclusions imbedded in a matrix and can be extended to periodic composites with three or more phases, the discussion will be restricted to two-dimensional structures such as those shown in Fig. 1. The treatment is completely parallel to the theory of the band structure of solids[2] but it involves vector, rather than scalar, wave functions. Another analogy may be drawn with the vibrations of a crystal lattice, with the difference that the composite is a continuous medium rather than a lattice of point masses coupled by springs.

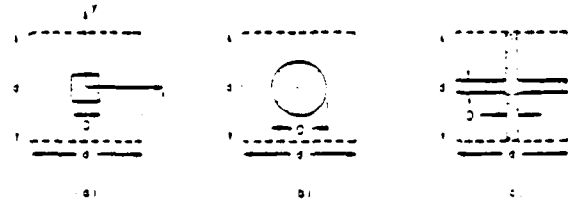

Figure 1 — Two-dimensional composite unit cell geometries.

In a homogeneous elastic medium, where the elastic constants and density are spatially constant, wave propagation at frequency ω is governed by

$$c_{ijkl}\,u_{k,lj} = -\rho\omega^2 u_i$$

where the ∂_j-derivative actually appears to the left of the elastic constant but can be shifted to the right-hand side when the constant is uniform in space. This step cannot be taken in a composite, where spatial derivatives of the elastic constants must be considered. To do this, it is convenient to write Eq. (1) as

$$\partial_{II}c_{IJ}\partial_{Jj}u_j = -\rho\omega^2 u_i \quad , \qquad (2)$$

where the operators are defined in Ref. 3, and to separate the material parameters into spatial average and spatially varying parts,

$$c_{IJ}(x,y) = \bar{c}_{IJ} + \Delta c_{IJ}(x,y) \quad , \qquad (3a)$$

$$\rho(x,y) = \bar{\rho} + \Delta\rho(x,y) \quad . \qquad (3b)$$

Substitution reduces Eq. (2) to

$$(\bar{\underline{\underline{\Gamma}}} + \bar{\rho}\omega^2\underline{\underline{I}}) \cdot \underline{u} = \underline{\underline{P}}(x,y) \cdot \underline{u} \quad , \qquad (4)$$

a 3 × 3 matrix equation. The first term on the left is the operator on the left-hand side of Eq. (2), written for the spatial average elastic constants, and the second term is proportional to the identity matrix. On the right,

$$\underline{\underline{P}}(x,y) = -(\Delta\underline{\underline{\Gamma}} + \Delta\rho\omega^2\underline{\underline{I}}) - \underline{\underline{I}} \quad , \qquad (5)$$

where the quantity in parentheses has the average constants appearing in the left-hand side of Eq. (4) replaced by the spatially varying values in Eq. (3). The second term takes account of the spatial derivatives of the elastic constants. It has the form

$$\text{Diagonal} \rightarrow \begin{matrix} (\partial_x c_{11})\partial_x + (\partial_y c_{44})\partial_y \\ (\partial_y c_{11})\partial_y + (\partial_x c_{44})\partial_x \\ (\partial_x c_{44})\partial_x + (\partial_y c_{44})\partial_y \end{matrix} \quad , \qquad (6a)$$

$$\text{Upper Offdiagonal} \rightarrow \begin{matrix} (\partial_x c_{12})\partial_y + (\partial_y c_{44})\partial_x \\ (\partial_x c_{12})\partial_z \\ (\partial_y c_{12})\partial_z \end{matrix} \quad , \qquad (6b)$$

with the lower offdiagonal elements obtained by interchanging ∂_x and ∂_y.

By analogy with the Floquet-type solution of Brillouin,[4] the general solution [illegible] is written in the form of a summation [illegible] space harmonics

$$\underline{u} = \sum_{lm} \underline{a}_{lm} e_{lm} \exp - i\underline{\beta}_{lm} \cdot \underline{r} \quad ,$$

with space harmonic wave vectors

$$\underline{\beta}_{lm} = \hat{x}(\beta_x + 2\pi l/d) + \hat{y}(\beta_y + 2\pi m/d) + \hat{z}\beta_z \qquad (7b)$$

For conciseness, summation signs are omitted and summation over repeated subscripts is understood. The first two subscripts in Eq. (7a) are integers ($-\infty$ to $+\infty$) describing the order of the space harmonic and the third subscript n is a vector polarization label. Since each space harmonic (lm) is a three-dimensional vector field it must be described by three vector components. These could be taken as components with respect to the coordinate axes. However, it is much more useful to take as a basis the polarization vectors of elastic waves propagating in the <u>average</u> medium with wave vector β_{lm}. Only isotropic media will be considered here and, in this case, the decomposition is as shown in Fig. 2. This means that

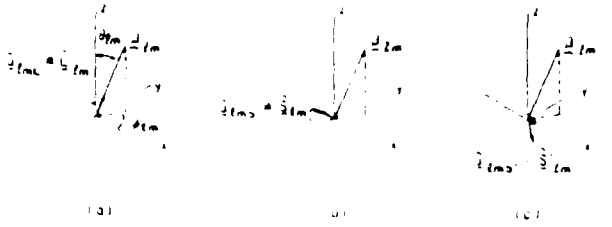

Figure 2 — Vector space harmonics of order lm for a periodic elastic composite. (a) Longitudinal polarization. (b) Vertical shear polarization. (c) Horizontal shear polarization.

the polarization vectors in Eq. (7a) are eigenvectors of the left side of Eq. (4). Because of this, Eq. (4) reduces to an infinite set of coupled equations for the space harmonic amplitudes

$$\bar{\rho}\omega^2 - \bar{\Gamma}_{ijkl}\beta_{lm}^2 a_{lmn} = \kappa_{lmn,pqd} a_{pqd} \quad , \qquad (8)$$

where the [illegible] on the left-hand side are average elastic wave constants. The coupling constants are

$$\kappa_{lmn,pqd} = \frac{1}{A} \int_{\text{cell}} \underline{\underline{P}}(x,y) \cdot \underline{u}_{pqd} \, e^{i\underline{\beta}_{lm} \cdot \underline{r}} \, dA$$

[illegible]

[illegible] where the [illegible] in the second line is the

the square rod lattice of Fig. 1(a). For the circular rod geometry the sinc functions are replaced by sinc functions. A dispersion relation between ω and β_{z0} in Eq. (7b) is obtained by setting the determinant of Eq. (8) to zero, performed in practice by truncating the system and adding additional terms until satisfactory accuracy is attained. In the limit of $D = 0$ in Fig. 1 the coupling constants go to zero, and the solutions become the three plane elastic solutions traveling in the direction of β_{z0} in a homogeneous medium. Consequently, the solutions (elastic Bloch waves) of Eq. (8) are of three distinct types, consistent with this limiting behavior.

3. Wave Propagation in Special Directions

Understanding the wave behavior described by the theory above and applying it to the interpretation of experiments is facilitated by considering special propagation directions. If β_z is zero in Eq. (7b), the assumed solutions are z-independent and the matrices in Eq. (4) partition into a 2×2 matrix involving u_x, u_y and a scalar part involving u_z. This is easily pictured physically if the generation of space harmonics is visualized as arising from multiple scattering of xy-propagating waves by a periodic square array of the z-oriented rods in Fig. 1; and it means that z-polarized (and xy-polarized) solutions can be treated independently.

The z-polarized solution, being scalar, has the same form as an electronic wave function and is therefore particularly useful for picturing the physical behavior of these waves. A basic feature is the existence of stopbands, which can be related to Bragg scattering from planes of rods having various orientations in the square lattice. The essential phenomena can be explained by reference to Fig. 3. Suppose in Fig. 3(a) that a z-polarized x-propagating shear wave is incident on the grating. At a frequency for which the rod spacing d is one-half shear wavelength, constructive reflection (Bragg scattering) occurs from the vertical planes

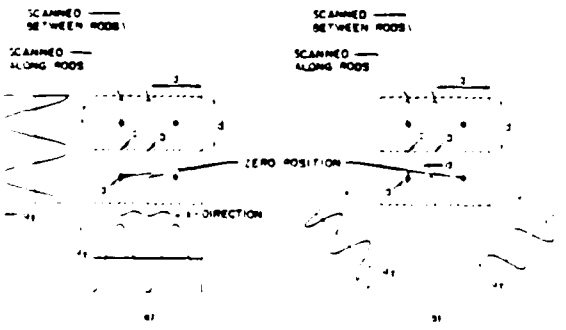

Figure 3 — Unit cell geometries and laser scan paths. (a) Standing waves at the second stopband, along the unit cell edge. (b) Standing waves at the second stopband, along the unit cell diagonal.

of rods, and resonance occurs between adjacent vertical planes. The x-propagating wave is also scattered from planes of rods at ±45 degrees to the x and y axes; but, in this case, Bragg conditions are not satisfied and resonance does not occur. A stopband exists at $d = \lambda_s/2$ for an x-propagating wave, but there is no resonant scattering into y-propagating waves. At the stopband edge the solution is a standing wave along x. If the scattering is weak, the wave form is accurately described by only two space harmonics, those for which the corresponding left-hand sides of Eq. (8) are simultaneously near resonance (0 0 and -1 0; with $\beta_{z0} \doteq \beta_x$). From the square symmetry of the lattice a similar standing wave solution along y, described approximately by space harmonics (0 0 and 0 -1; with $\beta_{z0} \doteq \beta_y$), also exists. This behavior corresponds to the first stopband of the lattice.

When the rod spacing d is one shear wavelength, a completely different standing wave pattern results, as illustrated in Fig. 3(a). In this case a z-polarized x-propagating wave is again Bragg scattered, with a phase shift of 2π from one vertical plane of rods to an adjacent plane. However, it is easily verified that the wave is also Bragg scattered, at the same frequency, by the ±45° planes of rods, so that resonant scattering of the x-propagating wave into a y-propagating wave occurs. These y-propagating waves also experience resonant scattering of the same type. As a result, the solution is a two-dimensional resonant standing wave pattern described, for weak scattering, by four space harmonics (0 0, -2 0, -1 1, -1 -1, with $\beta_{z0} \doteq \beta_x$). Different combinations occur, consistent with the symmetry of the lattice. Figure 3(a) shows the one for which the rods all vibrate in phase. This and the other two-dimensional standing wave patterns correspond to the second stopband of the square composite lattice.

Similar comments can be made for xy-polarized wave propagation, starting from an x-polarized x-propagating or a y-polarized x-propagating wave. In this case the Bragg scattering argument shows that only longitudinal space harmonics or shear space harmonics can be simultaneously near resonance, a conclusion that is easily confirmed by Eq. (8).

Another special case is the one for which

$$\beta_x = \beta_y = 0 \qquad (9)$$

in Eq. (7b). Suppose, for example, a z-polarized z-propagating wave is incident on the lattice. No Bragg scattering can occur because the structure is uniform along z. However, a spatial modulation of the phase fronts is produced by the difference in the properties of the rods and the matrix. Consequently, space harmonics are generated, but none are resonant. Similar conclusions are obtained for z-propagating waves of other polarizations, and all are consistent with the system of coupled space harmonic equations (Eq. 8).

VIII. APPENDIX B

LAMB WAVE FLOQUET THEORY FOR A PERIODICALLY COMPOSITE PLATE

Floquet theory for an infinite isotropic composite medium was formulated in Appendix A by expressing solutions to the acoustic wave equation in a series of plane wave harmonics. Each order of space harmonic (for example, the ℓm-th space harmonic) includes plane waves with the three possible plane wave polarizations corresponding to the space harmonic propagation factor $\underline{\beta}_{\ell m}$ (Fig. 2 of Appendix A). There are therefore three space harmonic amplitudes $a_{\ell m \eta}$ ($\eta = L, S, S'$) in each order (ℓm) of space harmonic. Substitution of the Floquet solution (or space harmonic expansion) into Eq. (2) of Appendix A, and use of the orthogonality properties of the space harmonic wave functions, lends to an infinite set of coupled equations for the space harmonic amplitudes (Eq. (8) in Appendix A). Standard methods can be used to solve these equations, including the coupled-wave approximation (in which only space harmonics that are near "resonance"—i.e., have the right-hand member of Eq. (8) near zero—are retained). Difficulties arise in treating the composite plate problem by this method, because space harmonics are coupled *both* by the spatial inhomogeneities ($\Delta\rho, \Delta c_{IJ}$) *and* by the plate boundary conditions. These boundary conditions couple not only space harmonics of different orders but also different polarizations in the same order of space harmonic. Selection of the important terms in the Floquet solution therefore becomes very complicated.

The difficulties stated above can be avoided by taking the space harmonic terms in the Floquet solution for the plate to be Lamb mode and SH mode wave functions, rather than combining infinite plane wave space harmonics to match the plate boundary conditions. By *choosing Lamb and SH mode* wave functions as a basis, one pre-matches the space harmonics to the plate boundary conditions. To illustrate the method, a simplest example (the one-dimensionally periodic composite plate of Fig. 4) has been chosen. For plate mode Floquet analysis the acoustic field equations

$$\begin{bmatrix} 0 & \nabla \cdot \\ \nabla_s & 0 \end{bmatrix} \begin{bmatrix} \boldsymbol{v} \\ \boldsymbol{T} \end{bmatrix} = i\omega \begin{bmatrix} \bar{\rho} & 0 \\ 0 & \bar{\boldsymbol{s}} \end{bmatrix} \begin{bmatrix} \boldsymbol{v} \\ \boldsymbol{T} \end{bmatrix} + i\omega \begin{bmatrix} \Delta\rho & 0 \\ 0 & \Delta\boldsymbol{s} \end{bmatrix} \begin{bmatrix} \boldsymbol{v} \\ \boldsymbol{T} \end{bmatrix} \tag{1}$$

are used, rather than Eq. (1) of Appendix A. Here, the spatial average density $\bar{\rho}$ and compliance $\bar{\boldsymbol{s}}$ are defined in a similar way to $\bar{\rho}$ and $\bar{\boldsymbol{c}}$ of Appendix A. The general form of the Floquet solution is

$$\begin{bmatrix} v \\ T \end{bmatrix} = \begin{bmatrix} v(z) \\ T(z) \end{bmatrix} \exp(-i\beta_0 x)$$

$$= \sum_n a_n \begin{bmatrix} v_n(z) \\ T_n(z) \end{bmatrix} \exp(-i\beta_n x) \tag{2}$$

$$\beta_n = \beta_0 + 2\pi n/d ,$$

where $v(z)$, $T(z)$ are functions of period d (expanded in a Fourier series), and a_n are the space harmonic amplitudes. At the stress-free surfaces of the plate ($z = 0, b$) the boundary conditions are

$$\hat{z} \cdot T = \sum_n a_n \hat{z} \cdot T_n \exp(-i\beta_n x) .$$

Since this condition applies for all values of x,

$$\hat{z} \cdot T_n = 0 \tag{3}$$

for all n.

As in Appendix A, the individual space harmonic wave functions on the right-hand side of Eq. (2) must be expanded in suitable basis functions. In a structure with one-dimensional periodicity and propagation parallel to the periodicity, the Lamb and SH modes are decoupled by symmetry. The Floquet solutions may therefore be taken to be of either Lamb mode or SH mode species. Here, the first case is chosen; and

$$a_n \begin{bmatrix} v_n(z) \\ T_n(z) \end{bmatrix} \exp(-\beta_n x) = \sum_\nu a_{n\nu} \begin{bmatrix} v_{n\nu}(z) \\ T_{n\nu}(z) \end{bmatrix} \exp(-i\eta_n x) , \tag{4}$$

where $v_{n\nu}$, $T_{n\nu}$ is the Lamb mode function that satisfies the acoustic field equations at β_n and $\omega = \omega_{n\nu}$ (Fig. 4). These mode functions can be shown to satisfy the orthogonality condition of Eq. (11.75) in Reference 5. To develop coupled space harmonic amplitude equations, Eq. (4) and Eq. (2) are substituted into Eq. (1). This result is reduced to a set of coupled space harmonic equations by following the procedure used in deriving Eq. (11.71) of Reference 5 (taking solution "1" to be Eq. (2) above and solution "2" to be the Lamb mode wave function with $n = m$ and $\nu = \mu$ ($\omega = \omega_{m\mu}$) in Eq. (4). The result, corresponding to Eq. (11.71), is then integrated through the plate thickness. Expanding the divergence operator on the right-hand side of Eq. (11.71), applying the boundary conditions of Eq. (3), using the fact that the m, μ solution satisfies the field equations at $\omega = \omega_{m\mu}$, and integrating over the unit cell, finally yields the coupled space harmonic equations

$$(\omega - \omega_{m\mu}) a_{m\mu} = \omega \sum_{n\nu} K_{m\mu,n\nu} a_{n\nu} . \tag{5}$$

The coupled constants on the right-hand side of Eq. (5) are obtained by integrating the $\Delta\rho, \Delta s$ matrix in Eq. (1) (weighted by multiplying with appropriate combinations of Lamb mode space harmonic functions) over the unit cell of the composite.

IX. PRESENTATIONS

H. Kunkel presented Reference 8 in Section VI at the IEEE International Symposium on APPLICATIONS OF FERROELECTRICS (ISAF), Gaithersberg, Maryland, May 1983.

T.R. Gururaja presented Reference 1 at the 5th European Meeting on Ferroeletricity, Benalmadena (Malaga), Spain, September 1983.

A. Maradudin presented Reference 2 on our behalf at the International Conference on the Dynamics of Interfaces, Lille, France, September 1983.

B.A. Auld presented References 3 and 9 at the 1983 IEEE Ultrasonics Symposium, Atlanta, Georgia, November 1983.

B.A. Auld described the Floquet theory of periodic composites at the Penn State Materials Research Laboratory review presentation on Targeted Basic Studies of Ferroelectric and Ferroelastic Materials for Piezoelectric Transducer Applicaions, November 1983.

X. PUBLICATIONS AND PATENT DISCLOSURES

References 1, 2, 3, 8, 9.
Patent Disclosure: Acoustic Interface Waveguide Directional Coupler, April 1984.

XI. PERSONNEL

Principal Investigator: B. A. Auld
Visiting Scientist: Y. A. Shui, Nanjing University, China (left in June 1983).
Graduate students: H. A. Kunkel (degree expected Fall 1984); Y. Wang; G. Laguna (Sandia Fellowship).

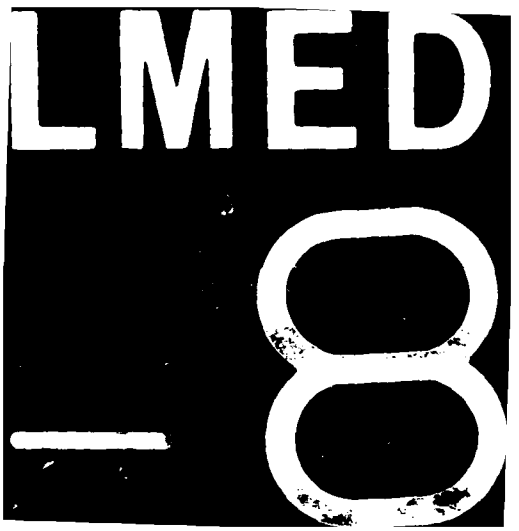
LMED
8